École polytechnique de Louvain

DC microgrid load flow analysis for electric vehicles loads

Author: **Antoine van Cutsem**
Supervisors: **Emmanuel De Jaeger, Eduardo Vasquez Mayen**
Reader: **Marc Bekemans**
Academic year 2023–2024
Master [120] in Electro-mechanical Engineering

Acknowledgements

I would like to express my deepest gratitude to my supervisor, Professor Emmanuel De Jaeger and my co-supervisor PhD candidate Eduardo Vasquez Mayen for their guidance and knowledge throughout the course of this research. Their feedback and suggestions have helped me refine my ideas and improve the overall quality of this thesis. Above all, I would like to thank you for the availability you have shown towards me and the great communication we have had throughout the year.

Finally, I would like to thank Professor Marc Bekemans for accepting his role as reader and jury member.

Thank you for your time and effort, all three of you.

Finally, I would like to thank my family for allowing me to undertake these studies and to see them through to the end with this work, which is the culmination. Thank you to them for their support and patience during the pressure-packed moments of this journey.

Abstract

This thesis examines the role of microgrids in moderating the additional stress put on the electrical grid caused by the growing share of renewable energy sources and the electrification of our society as part of the fight against climate change and the need for decarbonization.
By coupling a stochastic model based on practical data with a linearized load flow model, this work has developed an algorithm capable of efficiently simulating various DC microgrid architectures. They constitute the base cases from which scenarios are developed by adding charging stations for electric vehicles, allowing their impact on the microgrids to be studied through a load flow analysis. This study, together with forecasts of the challenges these systems will face in 2030 as a result of Belgian policy on company cars, enables conclusions to be drawn about their future and the main objectives of this thesis.
Key findings suggest that current existing microgrids are not well-suited to accommodate this increased fleet of electric vehicles and their performance will diminish unless an unrealistic area is dedicated to photovoltaic production. Significant variations in the results indicate the importance of carefully planning the integration strategy for electric vehicle charging stations and the difficulty of drawing unanimous conclusions for every possible architecture.

Table of abreviations

GHG	Greenhouse Gases
CO2	Carbon dioxide
EV	Electric Vehicle
RES	Renewable Energy Sources
MG	Microgrid
DER	Distributed Energy Resources
DC	Direct Current
PV	Photovoltaic
AC	Alternating Current
DCMG	Direct Current Microgrid
EVCS	Electric Vehicle Charging Station
CC	Constant Current
CV	Constant Voltage
CP	Constant Power
IEC	International Electrotechnical Commission
SOC	State Of Charge
CDF	Cumulative Distribution Function
PDF	Probability Density Function
CR	Constant Resistance
DG	Distributed Generation
MPPT	Maximum Power Point Tracking

POC Point Of Connection

SCI Self-Consumption Index

SSI Self-Sufficiency Index

Contents

List of Figures

List of Tables

Introduction

Background

Climate change is one of the most pressing challenges facing humanity requiring adaptation and innovation from all humankind. The increasing emissions of greenhouse gases (GHG), particularly carbon dioxide (CO2) since the beginning of the industrial era due to the burning of fossil fuels is identified as the main reason for this global crisis. Among the various contributors to CO2 emissions, the transportation sector stands out as a significant player, reaching close to 22% of global emissions [1].

The solution that has been brought to tackle this sector as many others is the electrification of it preventing the additional direct release of CO2 due to the traditional combustion engines. By transitioning from conventional gasoline-powered vehicles to electric vehicles (EVs), additional stresses are put on the electric grid due to the increase in loads that it brings with it. The increasing share of renewable energy sources (RES) and the green electricity that it allows to produce has further lightened the environmental footprint of global mobility while simultaneously intensifying the instability of the grid because of the intermittency due to their reliance on weather conditions.

In response to these challenges, decentralized and distributed generation systems have become more and more popular. Microgrids (MGs), in particular, have emerged as a viable solution to enhance grid reliability, energy efficiency, and resilience. This localized and small-scale energy system is constituted of several loads and distributed energy resources (DERs) and can operate autonomously or in conjunction with the main grid. This decentralized approach enables efficient management of electricity generation, consumption, and storage within a defined geographical area.

Moreover, additional studies are made about this new concept with the idea of implementing it in direct current (DC) as many modern loads like batteries and EVs consume DC power and photovoltaic panels (PV) produce DC power [2].

The main advantage that lies behind it is the easy integration of those consumption and generation sources without requiring the conversion from DC to alternating current (AC) power and conversely allowing to decrease the losses it implies and the costs inherent to the purchase of inverters and rectifiers.

This thesis focuses on the analysis of DC microgrid load flow, with a specific emphasis on electric vehicle loads. More specifically, it's based on a linear power flow method for droop-controlled DC microgrids [3] and studies the voltage and current quality and other variables by modifying several independent parameters to measure their impact. Comparisons of cases with and without EVs are made to highlight their effect on the MG.

Microgrid

Microgrids were born out of the need for DERs because of the growing share of RES to deal with global warming. They enhance power system reliability, reduce grid stress, and promote renewable energy integration. They are small-scale, localized, low-voltage networks that can operate in AC or DC. The choice of implementation depends on the share of the load and the resulting economic benefit. In the context of this work, a DCMG was chosen because the loads are mainly DC loads, which avoids the additional costs due to losses and the purchase of converters.

Characterized by distributed generators, energy storage systems, and telecommunication elements, MGs operate either connected to or independently from (islanded mode) larger grids. In islanded mode, the MG regulates power quality itself by balancing consumption and production at all times. When the MG is connected to the main grid, the voltage is set by the connection point. There is at least one point of connection with a larger electrical grid that can be triggered depending on the equilibrium of the MG. The generation and consumption loads present in the MG studied in this paper consist of industrial loads, photovoltaic generation, batteries and EV charging stations (EVCS).

The main advantages of MGs are the reduced dependence on the main grid, the ease of integrating new resources, the ease of increasing or decreasing capacity and the equitable role of each resource in determining the operation of the MG.

In short, MGs show great potential as efficient and reliable solutions for meeting our energy needs, relieving pressure on the grid and promoting the integration of renewable energy sources. With their intelligent control strategies, simplified installations and focus on maintaining power quality, they are well-equipped to meet today's energy challenges and support the transition to sustainable energy.

Motivation

In light of the considerations mentioned in Background, it is clear that direct current microgrids (DCMGs) are a relevant concept to explore and can constitute a powerful tool against climate change. Despite all the advantages they present, DCMGs are facing many challenges that need to be studied and well understood.

Although a lot of research on power flow analysis of a traditional AC grid has been conducted, few have been done on DCMGs. In addition, those that have been carried out are often based on incomplete or too sophisticated techniques. The one used for this thesis presents the advantages of considering the droop control aspects and of simplifying the non-linear algebraic equation by linearizing them resulting in a far smaller computation time and has proven to keep a good precision [3].

This thesis stands out by the fact that it features a realistic simulation of a MG by implementing industrial loads and plausible stochastic load profiles of electric vehicle charging stations (EVCS) as well as power production based on collected irradiance data and photovoltaic panels. It is a macro study of several independent assets that goes thoroughly through the problem and observes the behaviour of the MG depending on its interconnection with the main grid.
Additionally, it goes beyond a simplistic power-oriented perspective by considering the different phases of EV charging, including constant current (CC) and constant voltage (CV) modes.

Finally, given the current regulatory landscape, which incentivizes the adoption of EVs through fiscal advantages and mandates the transition to 100% EV company cars by 2030, it becomes increasingly pertinent to study their impact on the grid, especially within the context of a MG.

Research questions and objectives

The following research questions clarify the objectives that this thesis aims to achieve and give a common thread to follow.

- What are the electric vehicles' charging dynamics ?

- What is the impact of integrating an EV charging station into a DCMG ?

- How does the DCMG react to variations in parameters that can be considered as changes in people's social behaviour such as arrival and departure times, vehicle size, carpooling, etc ?

- What is the effect of different kinds of architecture on the DCMG (number of nodes, location of the nodes, distribution of the share of the load/production, etc) ?

Thesis structure outline

This thesis is organized into several chapters and sections:

Chapter 1 provides readers with the necessary background to understand EV charging to have sufficient comprehension of it for the coming discussions. It delves into various charger technologies, power modes and sources. Moreover, it explores battery cell dynamics and defines the one used in this paper.

Chapter 2 describes the two models employed in this thesis that have been combined to carry out this study. It explains the purpose of each model while providing a clear and brief overview. Their literature review has been resumed to put in context why they have been chosen for this work. Additionally, their limitations are exposed and the modifications made to adapt them to the objectives of the thesis are cited.
Finally, the novelty of this work is mentioned. It is also based on a literature review of what already exists but focuses more on the subject of this thesis.

Chapter 3 exposes the methodology and scenarios utilized to obtain the results.
First, some are aimed at understanding the behaviour of the DCMG and its responses to variations. Then, a specific case is chosen to illustrate the difference between CC and constant power (CP) load and the interest of studying them separately. Scenarios that allow to isolate the impact of EVCS are presented, followed by forecasts for the year 2030.

Chapter 4 presents and discusses the simulation results. They are separated in the same way as the scenarios to highlight the different results targeted. Most of the time, comparisons are made against the base case or other relevant scenarios.

Chapter 5 concludes the thesis by summarizing key findings and lessons learned. It also suggests future work ideas that could be done based on the outcomes of this work.

Chapter 1

Electric vehicles charging

This chapter is an introduction to EV charging operations. More precisely, there are three main EV charging methods which are: conductive charging, inductive charging and battery swapping. This section focuses on the first one and aims to provide comprehensive insights necessary for a proper understanding of this thesis. The content is strongly based on the paper of Veneri et al. [4].

1.1 The electric vehicle

Before delving into the specifics of EV charging, it is important to understand the different types of existing electric vehicles.
In the broadest sense, the term EV refers to a vehicle that runs at least partially on electricity. It encompasses a range of different types of EVs that have been created and are classified in the following list [5].

EV (Electric Vehicle) also called BEV (Battery Electric Vehicle) is exclusively powered thanks to electricity which is stored in a battery.

HEV (Hybrid Electric Vehicle) has both a combustion and an electric engine. They can't be plugged in to recharge so the battery is replenished through regenerative braking or deceleration.

PHEV (Plug-in Hybrid Electric Vehicle) is an HEV but with the added benefit of being able to charge the electric battery while connected to an electric socket or charger. They have a larger battery.

FCEV (Fuel Cell Electric Vehicle) is an EV in which electricity is produced thanks to hydrogen which is stored. It requires less charging than a conventional EV.

EREV (Extended Range Electric Vehicle) is similar to PHEV but the combustion engine is only used to charge the electric battery.

1.2 AC vs DC charging

Conductive charging of EVs distinguishes itself from the two other methods by the fact that electricity is brought to the vehicle through a cable connected to an electric socket. Then we can distinguish two kinds of charging: AC charging and DC charging. The saying of AC charging isn't completely right as batteries are supplied in DC so it always occurs technically in DC. It serves to know which type of current is going through the cables and where the conversion occurs.

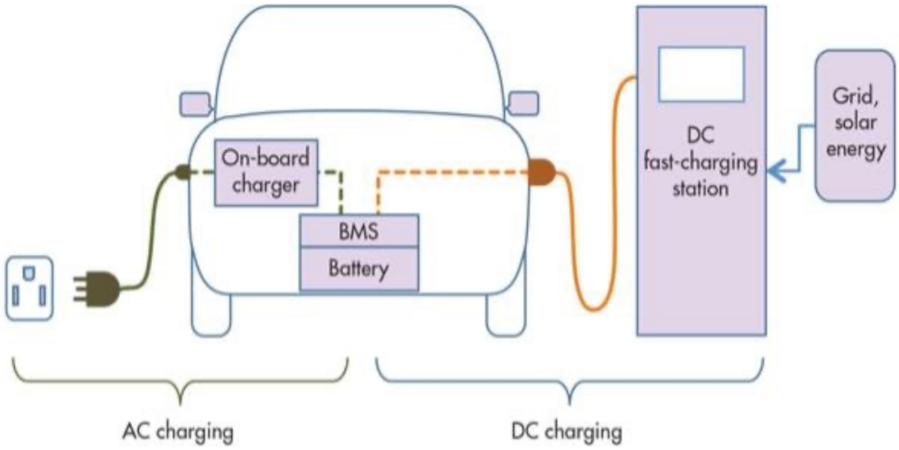

Figure 1.1: AC vs DC charging [6]

Figure 1.1 highlights the fact that in AC the inverter is in the vehicle so the conversion is taking place on board while for DC charging, the inverter and the conversion are off board. The rationale behind that lies in the fact that as previously said batteries are fed in DC and the traditional grid is fed in AC which means that a conversion is necessary and it is not wanted to have a big and heavy inverter inside a car.
In comparison, for DC charging, the conversion takes place outside such that a massive inverter can be placed as shown. This off-board inverter can handle the conversion of important power while the small ones inside vehicles can only accept a moderate amount of power. That explains why DC charging is often referred to as fast charging.

1.3 Charging modes

Conductive charging speed and infrastructures are classified into four charging modes as defined by the International Electrotechnical Commission (IEC) Technical Standard

61851 [7].
The first three modes are directly connected to the AC supply network which means that conversion is taking place on board while the last mode is indirectly connected such that the vehicle is charged via an external charger and the conversion occurrs off-board providing DC as explained in the previous section.

Mode 1 is the slowest charging mode. It uses a non-dedicated power socket, like a domestic socket, with a simple cable which implies a risk of overheating. The voltage and current do not exceed 250V in single-phase AC and 480V in three-phase AC, with a maximum current of 16A. It results in a maximum power of 4 kW for single-phase charging and 7.5 kW for three-phase charging.

Mode 2 is classified as slow charging. It's also charging via a non-dedicated power socket but through a cable with a communicating charge monitoring device. It's connected to the grid with the same voltage limit as mode 1 but with a maximum current of 32A resulting in a power limitation of 8 kW and 15 kW for single-phase and three-phase charging, respectively.

Mode 3 is a "semi-fast" charging solution where a dedicated cable and socket, which incorporates charge monitoring, are used. The same voltage limitations are applied, while the current can reach 63A. In this configuration, users can expect a maximum power output of 15.5 kW to 30 kW for their vehicle, depending on the current configuration.

Mode 4 is known as fast charging. The DC external charger embeds charge monitoring and utilizes a dedicated cable. The limitations vary depending on the cable used but generally imply a maximum voltage of 500 V and a maximum current of 400 A, i.e. a maximum power of 200 kW. However, more recent charging points offering up to 500 kW have recently been introduced [8].

The following figures summarize the security and specifications of each charging mode.

Charging Mode	Max Current per phase	Charging Time	Vehicle Battery Charger
Mode 1	16 A	4÷8 h	On Board
Mode 2	32A	2÷4h	On Board
Mode 3	63A	1÷2h	On Board
Mode 4	400 A DC	5÷30 min	Off Board

Figure 1.2: Charging mode specifications [4]

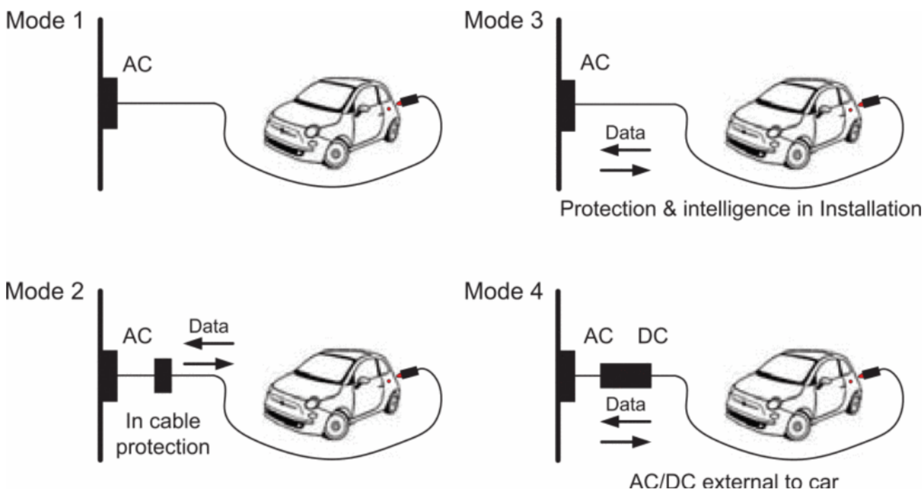

Figure 1.3: Schemes of the 4 charging modes[4]

Other factors influencing the vehicle's power supply include the charging station itself as well as the distance between them. As these charging stations represent a large amount of power, in some cases if many of them are used in the same location, the power supplied can be reduced to avoid deteriorating the stability of the grid. As previously mentioned, the choice of cable is important and paying attention to the specifications of the battery's car is also crucial.
For example, despite the *Tesla Model 3*'s similar battery size and higher peak power, it takes longer to charge than the *Kia EV6* which technically has a lower peak power capacity. The difference lies in the voltage of the batteries. The *Tesla Model 3* has a 400V battery while the *Kia EV6* has a 800V battery. By using Ohm and Joule's law [9], it appears that halving the voltages doubles the current while maintaining the power constant. Most importantly, it says that it quadruples the thermal losses. This explains why it can be seen on the fast charging curve of both vehicles in Figure 1.4 and Figure 1.5 that the *Tesla Model 3* isn't able to maintain its peak power for a long time.

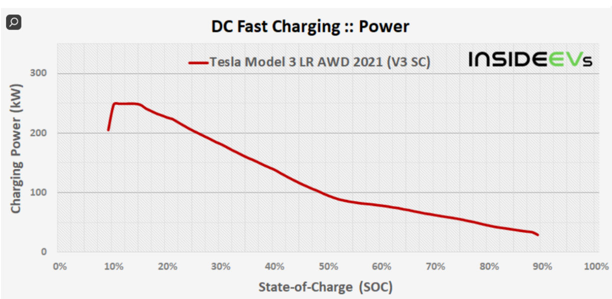

Figure 1.4: *Tesla Model 3* fast charging curve [10]

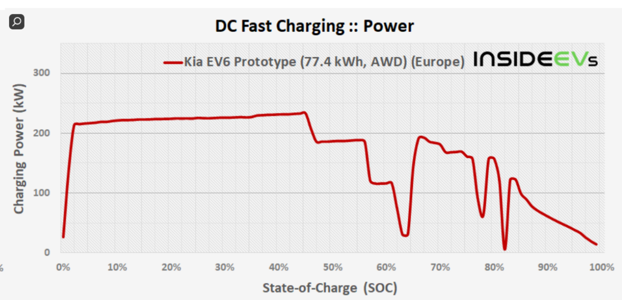

Figure 1.5: *Kia EV6* fast charging curve [11]

1.4 Battery cells

EV batteries are composed of battery cells arranged in parallel and series. There are various types of battery cells, each with its own specifications. They can differ in many features, such as their specific energy or charging rate.
They can also be distinguished by their charging profile as can be seen in Figure 1.6 and Figure 1.7 showing the power demand and related battery state-of-charge (SOC) profiles of a non-exhaustive sample of battery types.

The lithium-ion profile (on the right) is chosen for simulating the EV batteries used in this thesis. The plot highlights that for this type of battery, the power delivered is constant until the SOC reaches 90%.

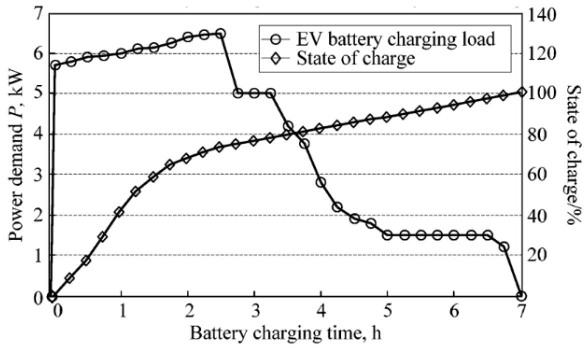

Figure 1.6: Lead-acid battery cell charging profile [12]

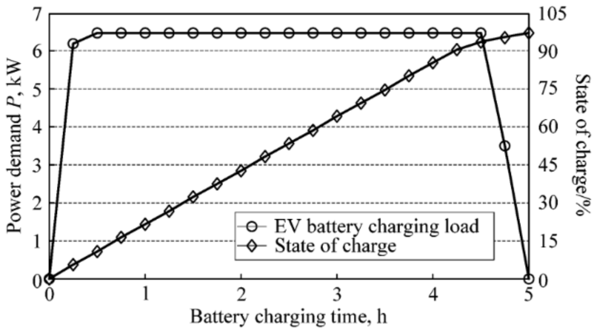

Figure 1.7: Lithium-ion battery cell charging profile [12]

Chapter 2

Model description

This chapter's goal is to provide a detailed explanation of the algorithm used to address the research questions of this thesis. It describes the two mathematical models upon which this thesis is based, explains their purposes and limitations in the context of this work and develops the modifications and assumptions made to adapt them to this study.
Once described, motivation and novel elements that this thesis brings are put in relief with the help of a state of the art on what led to the development of the two aforementioned models and the interest in combining them.
The details of the numerical values assigned to the parameters are discussed in chapter 3.

2.1 Stochastic model

A stochastic model was necessary for simulating the comings and goings of EVs and determining the associated power requirements at the charging stations of the MG while taking into account the randomness of several factors influencing it. Indeed, the outcomes depend on the variability of the inputs that define the probability distributions used for computations. These factors include the distribution of vehicle arrival and departure times, the initial mean and standard deviation of SOC, the types of EVs, commuting distances, penetration levels and charging modes.

2.1.1 Literature review

While various EV charging profiles exist, very few meet the specifications of this thesis. Many studies focus on domestic data [13], [14], so they can't be adapted to industrial/business applications or are based on AC grid [15], making them unsuitable for adaptation to DC applications due to factors such as the impact of reactive power

and phase angle.
Moreover, the dynamic nature of load behaviour is of great importance in the simulation of the results. Models that only provide daily analyses instead of hourly studies [16] or that only consider the energy required for the charging without accounting for power variations [17] aren't suitable for this thesis's purpose as they don't capture the rapid load fluctuations when working with charging stations or PVs.
In [12], Qian et al. proposed a promising model but it does not take into account the different charging modes. EV battery charging is generally separated into CC and CV modes which will be discussed in section 3.4. In [18], Marra et al. discussed this aspect but focused on a single vehicle rather than an aggregate.
The objective of this model is to predict daily EV load profiles while statistically separating the CC and CV portions for different deterministic values and stochastic distributions of the relevant factors mentioned above. The strength of this model lies in the fact that it is based on practical data collected at the University of Queensland.

2.1.2 Model overview

This subsection describes more shortly what is said in the document on which the stochastic model is based [19] to make it clear for the reader.

Arrival and departure of vehicles

The arrival (V_A) and departure (V_D) of vehicles are known which allows to determine the total vehicle present at the charging station (V_T) by using :

$$V_T(t) = V_T(t - T_s) - V_D(t) + V_A(t - T_S) \tag{2.1}$$

where T_S is the time step.

Arrival SOC

The distribution of arrival SOC, X_{Ai}, can be determined based on the normal distribution of the previous day's departure SOC, X_{PDDi}, and the normal distribution of driving distance between home and workplace, d_i. By using the following equations, the mean and variance of SOC on arrival, μ_{Ai} and σ^2_{Ai}, can be computed.

$$\mu_{Ai} = \begin{bmatrix} 1 \\ -C_i/d_{Ri} \end{bmatrix}^T \begin{bmatrix} \mu_{PDDi} \\ \mu_{di} \end{bmatrix} \tag{2.2}$$

$$\sigma^2_{Ai} = \begin{bmatrix} 1 \\ -C_i/d_{Ri} \end{bmatrix}^T \begin{bmatrix} \sigma^2_{PDDi} & \rho_{1i}\sigma_{PDDi}\sigma_{di} \\ \rho_{1i}\sigma_{PDDi}\sigma_{di} & \sigma^2_{di} \end{bmatrix} \begin{bmatrix} 1 \\ -C_i/d_{Ri} \end{bmatrix} \tag{2.3}$$

Where ρ_{1i} is the correlation coefficient between the previous day's SOC and driving distance, C_i is the choice factor of battery and d_{Ri} is the driving range of the vehicle. The choice factor of battery, C_i, is the percentage of the total distance covered using electric propulsion. It is less important for a hybrid vehicle than for a fully electric vehicle, which by definition is 100%.

Departure SOC

Considering that the probability of any vehicle leaving the charging station during the period between each time step is equal, it implies that removing $V_{Di}(t)$ number of vehicles at time t doesn't impact the distribution of SOC of the remaining cars. The vehicles arriving during this interval have the SOC distribution as described by the previous equation. Taking that into account, the normal distribution of the overall SOC at time t^-, $X_i(t^-)$, is identical to the departure SOC at time t, $X_{Di}(t)$, and the following relations can be established.

$$\mu_i(t) = \mu_i(t^-) = \mu_{Di}(t)\ ;\ \sigma_i^2(t) = \sigma_i^2(t^-) = \sigma_{Di}^2(t) \tag{2.4}$$

Finally, it can be determined as in Equation 2.5 and Equation 2.6.

$$\mu_i(t^-) = \begin{bmatrix} V_{TN}(t^-) \\ V_{DN}(t) \end{bmatrix}^T \begin{bmatrix} \mu_i(t^-) \\ \mu_{Di}(t) \end{bmatrix} \tag{2.5}$$

$$\sigma_i^2(t^-) = \begin{bmatrix} V_{TN}(t^-) \\ V_{DN}(t^-) \end{bmatrix}^T \begin{bmatrix} \sigma_i^2(t^-) & \rho_{2i}\sigma_i(t^-)\sigma_{Di}(t) \\ \rho_{2i}\sigma_i(t^-)\sigma_{Di}(t) & \sigma_{Di}^2(t) \end{bmatrix} \begin{bmatrix} V_{TN}(t^-) \\ V_{DN}(^-) \end{bmatrix} \tag{2.6}$$

Where $V_{TN}(t^-) = V_T(t^-)/(V_T(t^-) - V_D(t))$, $V_{DN}(t^-) = -V_D(t)/(V_T(t^-) - V_D(t))$ and ρ_{2i} is the correlation coefficient between the SOC at time t^-, $X_i(t^-)$, and the SOC of the departing vehicles, $X_{Di}(t)$.

After adding $V_A(t - T_S)$ and removing $v_D(t)$ at time t, the normal distribution of the overall SOC at time t^+ ($X_i(t^+)$) can be determined using Equation 2.7 and Equation 2.8.

$$\mu_i(t^+) = \begin{bmatrix} V_{TN}(t) \\ V_{AN}(t) \end{bmatrix}^T \begin{bmatrix} \mu_i(t) \\ \mu_{Ai}(t) \end{bmatrix} \tag{2.7}$$

$$\sigma_i^2(t^-) = \begin{bmatrix} V_{TN}(t) \\ V_{AN}(t^-) \end{bmatrix}^T \begin{bmatrix} \sigma_i^2(t) & \rho_{3i}\sigma_i(t)\sigma_{Ai}(t) \\ \rho_{3i}\sigma_i(t)\sigma_{Ai}(t) & \sigma_{Ai}^2(t) \end{bmatrix} \begin{bmatrix} V_{TN}(t) \\ V_{AN}(^-) \end{bmatrix} \tag{2.8}$$

$V_{TN}(t) = V_T(t)/(V_T(t)+V_A(t))$, $V_{AN}(t) = V_A(t)/(V_T(t)+V_A(t))$ and ρ_{3i} is the correlation coefficient between the SOC at time t, $X_i(t)$, and the SOC of arriving vehicles, $X_{Ai}(t)$.

Knowing this distribution and the number of vehicles present at the charging station, the demanded power can be computed and separated into CC and CV loads. The paper on which this model is based [19] uses the criterion specified by BS EN 61851-23:2014 [20] to segregate CC and CV loads. It defines the following :

$$CC : 0\% \leq SOC \leq 80\% \; ; \;\; CV : 80\% \leq SOC \leq 100\% \tag{2.9}$$

The different ways the power is computed are defined in the following equations :

$$\begin{gathered} \Delta X_{90i}(t) = S_{Bi}A_i(\Phi_i(t,100) - \Phi_i(t,90)) - \\ S_{Bi}B_i(\mu_i(t)(\Phi_i(t,100) - \Phi_i(t,90)) - \sigma_i^2(t)(\phi_i(t,100) - \phi_i(t,90))) \end{gathered} \tag{2.10}$$

$$P_{CC}(t) = s_i(t)P_{Ci}KM_i(1 - Q(\frac{80 - \mu_i(t)}{\sigma_i(t)})) \tag{2.11}$$

$$P_{CV80}(t) = s_i(t)P_{Ci}KM_i(Q(\frac{80 - \mu_i(t)}{\sigma_i(t)}) - Q(\frac{90 - \mu_i(t)}{\sigma_i(t)})) \tag{2.12}$$

$$P_{CV90}(t) = \frac{s_i(t)S_{Bi}KM_i\Delta X_{90i}(t)}{100T_s} \tag{2.13}$$

$$P_{CV}(t) = P_{CV80}(t) + P_{CV90}(t) \tag{2.14}$$

$$P_T(t) = P_{CV}(t) + P_{CC}(t) \tag{2.15}$$

where S_{Bi} is the size of the battery $[kWh]$, A_i and B_i are the battery-specific constants, Φ_i and ϕ_i are respectively the cumulative distribution function (CDF) and the probability density function (PDF) of X_i, K is the penetration of EV, M_i is the market share of the different vehicles, $s_i(t)$ is the charging set-point or charging efficiency in percentage, P_{Ci} is the charging power and $Q(x_i)$ is the error function of X_i where $Q(x_i) = 1 - Pr(X_i \leq x_i)$.

The SOC distribution at time $t + T_S$ can finally be updated as in Equation 2.16 and the delivered SOC is computed by using Equation 2.17.

$$\mu_i(t + T_s) = \mu_i(t^+) + (1 - Q(\frac{90 - \mu_i(t)}{\sigma_i(t)}))\frac{T_S s_i(t) P_{Ci}}{0.01 S_{Bi}} + \Delta X_{90i}(t) \tag{2.16}$$

$$\Delta\mu_a(t) = \sum_{i=1}^{N_{VT}} M_i(\mu_i(t^-) - \mu_{Ai}(t)) \tag{2.17}$$

Methodology

Step 1: Input of start-up parameters and arrivals $V_A(t)$, departures $V_D(t)$ and total number of vehicles $V_T(t)$.

Step 2: Computation of arrival SOC distribution, $X_{Ai}(t)$, and actual mean at time t by using Equation 2.2 and Equation 2.3.

Step 3: Computation of departure SOC distribution, $X_{Di}(t)$ and actual mean at time t

by using Equation 2.5 and Equation 2.6.
Step 4: Computation of delivered SOC at time t as in Equation 2.17.
Step 5: Update the number of total vehicles at time t^+ and update their overall SOC distribution using Equation 2.7 and Equation 2.8.
Step 6: Computation of CC, CV, and total power during t to $t + T_S$ thanks to Equation 2.10 to Equation 2.15.
Step 7: Update SOC distribution at time $t + T_S$ by using Equation 2.16

2.1.3 Limitations of the model and adaptations made to suit the thesis

Only one modification has been implemented in the model to align it with the load flow model. The above-described model is designed for SOC levels ranging from 10% to 100% while the stochastic model used for this thesis is limited to levels ranging from 20% to 90%. Although this adaptation can be seen as a limitation, it doesn't present any significant drawbacks as it is based on logical reasoning and serves to simplify the model.

Setting a lower limit of 20% for the SOC poses no complication while the upper limit of 90% is based on practical considerations. It's unlikely that the average SOC of a large number of EVs will be less than 20% or more than 90%.
Moreover, it's preferable to restrict the range as charging or discharging beyond these limits is harmful to the battery's lifespan [18].

Limiting the model to this range simplifies the dynamic of the battery because it can be seen that up to 90% of SOC, the delivered power is constant as observed in Figure 1.7. Given this consideration and the fact that the model is based on the BS EN 61851-23:2014 criterion [20] to segregate CC and CV loads, the charging mode is considered as CC up to 80% and CP up to 90%.
In addition, this approach avoids the use of CV mode, which isn't defined in the load flow model and the parameters that define the evolution of the charging load beyond 90% aren't given.

Concretely, Equation 2.10 and Equation 2.13 can be removed such that Equation 2.14, which is now actually renamed $P_{CP}(t)$, is simply equal to Equation 2.12 and Equation 2.15 is finally equal to $P_{CV}(t) + P_{CP}(t)$. The part about $\Delta X_{90i}(t)$ can also be removed from Equation 2.16. The normal distributions have also been truncated such that they are defined between 20% and 90%.

Some details make the model a bit less accurate than it could be. The fact that it doesn't implement the self-discharge of batteries and the changing efficiency of the charge as a function of the SOC can be mentioned but they are negligible considering the overall model.

2.2 Load flow model

A load flow analysis is carried out to assess voltage differences and power losses in the MG. It also provides information on the power flowing through the transmission lines to and from the main grid. It solves a set of algebraic equations and ensures that they converge, meaning that the power system is operating within acceptable voltage and current limits. It uses various power system parameters, including line resistance, industrial and EV load demands and photovoltaic generation. This investigation is crucial for effectively planning, designing, operating, and optimizing the performance of the system.

2.2.1 Literature review

This subsection highlights the relevant features of the load flow model used for this thesis [3] and summarizes them. It fits perfectly this work as it is able to solve load flow in DC rather than in AC [21], it's not limited to DCMG that are connected to a stiff grid [22], [23] so it applies to islanded DCMG. It also distinguishes itself from studies that are only valid for radial configuration [24] or that don't account for the primary-level droop-control effect [25]. Finally, it has the advantage of solving a linear set of equations which simplifies and fastens the execution and it takes into account all the different load types CP, CC and constant resistance (CR).

2.2.2 Model overview

A concise overview of the content discussed in the paper [3] which describes the linear power flow used in this work is provided in this subsection to offer clarity and brevity to the reader.

Dispatchable distributed generation (DG) units

The power outputs of dispatchable generators are independent of weather conditions and can be controlled. Typically, dispatchable DG units in DCMGs operate in droop mode for autonomous power sharing. While several technologies can serve as dispatchable DGs for DCMGs, this thesis focuses only on batteries. The point of connection with the main AC grid functions also as a dispatchable DG unit and can also operate using droop control. According to the droop operating characteristic, the current injected by the generator is influenced by the bus voltage. It means that a lower

bus voltage results in a higher current as depicted in Figure 2.1.
Equation 2.18 describes the phenomenon explained in the previous paragraph about dispatchable units.

$$V_i = V_{0i} - Rd_i I_i \tag{2.18}$$

V_i and V_{0i} are the bus voltage and no-load voltage reference, Rd_i is the droop value and I_i is the current injected by the dispatchable unit.
From Equation 2.18, the current injection at the bus i can be written as follows :

$$I_i = \frac{V_{0i} - V_i}{Rd_i} = (V_{0i} - V_i)Kd_i \tag{2.19}$$

where $Kd_i = 1/Rd_i$.

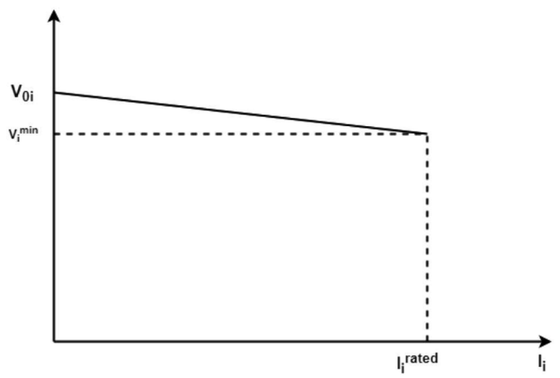

Figure 2.1: Droop control in a DCMG [3]

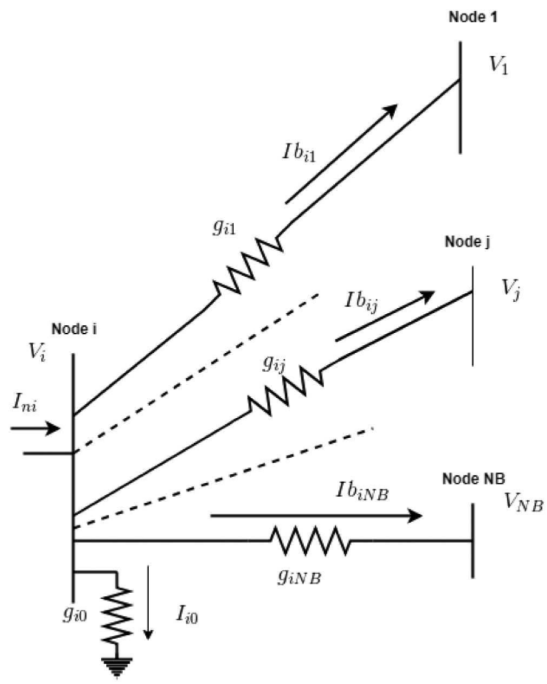

Figure 2.2: DC network [3]

Non-dispatchable DG units

Non-dispatchable or renewable DG units are reliant on weather conditions. Renewable units generally operate in maximum power point tracking (MPPT) mode to maximize energy production from natural sources. As a result, they are often not droop-controlled and inject CP according to weather conditions. In the case of this thesis, the only non-dispatchable DG energy produced comes from PV panels and is modeled as a negative CP load. The irradiance data used to determine the output of the PV panels were supplied by the teaching staff and are based on practical data. The bus current resulting from their operation is described in Equation 2.20.

$$I_{ndgi} = \frac{P_{ndgi}}{V_i} \tag{2.20}$$

Load model

In a DC power system, loads can be classified as CP, CI or CR. The power absorbed by a CP load is not affected by the magnitude of the node voltage [26]. Conversely, the power absorbed by a CI load varies proportionally to the node voltage [26], while the power absorbed by a CR load varies quadratically with respect to the node voltage [26]. The composite load can be expressed as the sum of these three types of load and is described as follows :

$$PL_i = P_{Pi} + hP_{Ii}V_i + h^2P_{Ri}V_i^2 \tag{2.21}$$

where P_{Pi}, P_{Ii} and P_{Ri} are respectively the CP, CI and CR components of the bus load at the rated DCMG voltage V_{rated}. The parameter h represents the per unit of the rated system voltage and is calculated as $h = 1/V_{rated}$.
The load current expression at bus i is obtained immediately and is given as follows :

$$IL_i = \frac{P_{Pi}}{V_i} + hP_{Ii} + h^2P_{Ri}V_i \tag{2.22}$$

Network model

The DCMG is represented by a network of supply lines, where only the real component of the impedance is present in steady state. A G-bus matrix is constructed to represent the interconnectivity between the different nodes of the system, consisting of conductances instead of admittances. The relationship between nodal currents and nodal voltages is expressed as follows:

$$[\mathbf{I}] = [\mathbf{G}][\mathbf{V}] \tag{2.23}$$

where **I** is the nodal current matrix, **V** is the nodal voltage matrix and **G** is the system conductance matrix.
The diagonal elements G_{ij} of the bus conductance matrix represent the sum of all conductances connected to node i, while the non-diagonal elements of G_{ij} (where $i \neq j$) indicate the negative value of the conductance between nodes i and j.

Referring to Figure 2.2, which illustrates a DC network where g_{ij} represents the line conductance between nodes i and j and g_{i0} represents the shunt conductance at node i, the current injection I_{ni} can be determined as in Equation 2.24.

$$\begin{aligned} I_{ni} &= I_{i0} + Ib_{i1} + Ib_{ij} + Ibi_{NB} \\ &= V_i g_{i0} + (V_i - V_1)g_{i1} + (V_i - V_j)g_{ij} + (V_i - V_{NB}g_{iNB} \\ &= -g_{i1}V_1 + (g_{i0} + g_{i1} + g_{ij} + g_{iNB})V_i - g_{ij}V_j - g_{iNB}V_{NB}) \end{aligned} \tag{2.24}$$

It can be compressed as follows:

$$\begin{aligned} I_{ni} &= \sum_{j=1}^{NB} G_{ij}V_j \\ &= \sum_{j=1;j\neq i}^{NB} G_{ij}V_j + G_{ii}V_i \end{aligned} \tag{2.25}$$

where NB is the number of buses, $G_{ii} = g_{i0} + g_{i1} + g_{ij} + g_{iNB}$ and $G_{ij} = -g_{ij}$.

Overall system model

The node current injection for a system bus i connected to a dispatchable unit, a renewable unit and a composite load can be expressed as follows:

$$\begin{aligned} I_{ni} &= I_i + I_{ndgi} - IL_i \\ &= \frac{V_{0i} - V_i}{Rd_i} + \frac{P_{ndgi}}{V_i} - \frac{P_{Pi}}{V_i} - hP_{Ii} - h^2 P_{Ri} V_i \end{aligned} \tag{2.26}$$

By replacing the expression of I_{ni} in Equation 2.26 with what has been written in Equation 2.25, the following equation is obtained :

$$\sum_{j=1;j\neq i}^{NB} G_{ij}V_j + G_{ii}V_i = \frac{V_{0i} - V_i}{Rd_i} + \frac{P_{ndgi}}{V_i} - \frac{P_{Pi}}{V_i} - hP_{Ii} - h^2 P_{Ri} V_i \tag{2.27}$$

Linear approximation

It can be observed that Equation 2.26 is linear in V_i, except for the terms linked to the CP load and the renewable generator. The CP terms are approximated to linearize the equation, transforming the problem into a linear power flow model. Node voltages are expressed in per unit (pu) in this work such that under normal operating conditions, the bus voltage generally remains within ±10% of the nominal value of 1.00 pu. The node voltage V_i can therefore be expressed as follows :

$$V_i = 1 - \Delta V_i \tag{2.28}$$

where ΔV_i is the deviation from the node voltage reference value.

To exploit the fact that the non-linear terms in Equation 2.26 have V_i in the denominator, the following function is defined and the Taylor series around zero is developed, which is analytical for all $|\Delta V_i \neq 1|$;

$$\Phi(\Delta V_i) = \frac{1}{V_i} = \frac{1}{1 - \Delta V_i} \tag{2.29}$$

$$\frac{1}{1 - \Delta V_i} = \sum_{k=0}^{\infty} (\Delta V_i)^k = 1 + \Delta V_i + (\Delta V_i)^2 + ... \tag{2.30}$$

If the node voltage is 0.90 pu, the value of ΔV_i is 0.10. Similarly, the value of the term ΔV_i^2 is 0.01. The other higher-order terms are even smaller and can be neglected without significant loss of accuracy. Therefore, neglecting the higher order terms, Equation 2.30 is reduced to :

$$\frac{1}{1 - \Delta V_i} = 1 + \Delta V_i \tag{2.31}$$

Using Equation 2.28, the following equation can be written :

$$\frac{1}{1 - \Delta V_i} = \frac{1}{V_i} 1 + \Delta V_i = 2 - V_i \tag{2.32}$$

By injecting this result in Equation 2.26, the nodal current approximation can be written as in Equation 2.33.

$$I_{ni} = \frac{V_{0i} - V_i}{Rd_i} + (P_{ndgi} - P_{Pi})(2 - V_i) - hP_{Ii} - h^2 P_{Ri} V_i \tag{2.33}$$

By replacing the expression of I_{ni} obtained in Equation 2.25 in Equation 2.33, the following equation can be written :

$$\begin{aligned} &\sum_{j=1;j\neq i}^{NB} G_{ij} V_j + V_i (G_{ij} + Kd_i + P_{Pi} + P_{ndgi} + h^2 P_{Ri}) \\ &= V_{0i} Kd_i - 2(P_{Pi} - P_{ndgi}) - hP_{Ii} \end{aligned} \tag{2.34}$$

Algorithm

A set of NB linear equations are solved simultaneously to get the power flow solution as shown in Equation 2.34. No Jacobian computation is required since the equations are linear and the operation remains non-iterative if the limits of the converter/generator aren't exceeded. The algorithm which describes the operations and handles the current limits is described below.

Line data storage [nl x 3] : There is *nl* number of rows that correspond to the lines of the system and 3 columns for the transmit and receive node numbers and line resistors.

Bus data storage [nb x 7] : There is *nb* number of rows that correspond to the nodes in the DCMG. The first column stores node numbers, the second column stores non-dispatchable or CP generations, the third column stores CP load demand, the fourth column stores CI load demand, the fifth column stores CR load demand, the sixth column stores the no-load voltage reference value, and the seventh column stores the droop value. For CP or load buses, the droop value is set to infinity.

Variables used : The iteration count (IT), the maximum number of iterations (ITMAX) and the termination indicator (CONV) are among the variables used. The process is finished if CONV = 1. PG and Plim refer to production and the maximum power limit and VIOL counts the number of units that have exceeded their maximum power limit.

Listing 2.1: Algorithm of the proposed linear power flow.

```
IT = 0; CONV = 0; ITMAX = max_number_of_iterations;
Gbus = zeros(nb, nb);
for ii = 1:1:nl
    fb = linedata(ii, 1);
    tb = linedata(ii, 2);
    r = linedata(ii, 3);
    Gbus(fb, fb) = Gbus(fb, fb) + 1/r;
    Gbus(tb, tb) = Gbus(tb, tb) + 1/r;
    Gbus(fb, tb) = Gbus(fb, tb) - 1/r;
    Gbus(tb, fb) = Gbus(tb, fb) - 1/r;
end for
while IT < ITMAX & CONV = 0
    IT = IT + 1
    A = zeros(nb, nb);
    for ii = 1:1:nb
        Rd = busdata(ii, 7);
        V0 = busdata(ii, 6);
        Pp = busdata(ii, 3);
        PI = busdata(ii, 4);
        Pr = busdata(ii, 5);
        Pndg = busdata(ii, 2);
        for jj = 1:1:nb do
            if ii == jj
                A(ii,jj) = Gbus(ii,jj)+h**2*Pr+1/Rd-Pp+Pndg;
```

```
            else
                A(ii, jj) = Gbus(ii, jj)+h**2*Pr+1/Rd-2*(Pp-Pndg);
            end if
        end for
        B(ii, 1) = V0/Rd-h*PI-2*(Pp-Pndg);
    end for
    v = linsolve(A, B);
    VIOL = 0;
    for ii = 1:1:nb
        % Calculate PG(ii)
        if PG(ii) > Plim(ii)
            PG(ii) = Plim(ii);
            busdata(ii, 7) = inf;
            busdata(ii, 2) = busdata(ii, 2) + PG(ii);
            VIOL = VIOL + 1;
        end if
    end for
    if VIOL == 0
        CONV = 1;
    else
        CONV = 0;
    end if
end while
```

2.2.3 Limitations of the model and adaptations made to suit the thesis

No modifications have been made to the model and no limitations can be identified or at least none that could be detrimental in the context of this study. The only non-ideality is that it solves algebraic equations that have been linearized which introduces a small percentage of error. However as studied in the paper [3], it's negligible and this approach results in a better computational time.

It may be noted that no CR loads are introduced in the thesis such that some of the terms in the equations in the previous subsection are unnecessary. The CP loads are the industrial loads and the EV load which can also be a CI load depending on the vehicle's SOC as explained by the segregation criterion, see Equation 2.9. The only non-dispatchable unit present is the solar panel, which is represented by a negative CP load.

2.3 Novel elements of this work

The objective of this work is to further explore the DCMGs and more precisely to study the impact of EV charging stations on it. To do so, the two aforementioned models are combined. They were used to fulfill their role explained at the beginning of section 2.1 and section 2.2 and they were chosen for the reasons detailed in their literature review, subsection 2.1.1 and subsection 2.2.1. Assembling these 2 models has enabled to distinguish this work from many other existing works on load flow analysis. Indeed, many works exist but they are mainly focused on main grid load flow analysis [27], [28] or if they are suited for MG analysis, they are done in AC so not suitable for DCMG [27]–[31].

In [32] and [33], a power flow analysis for a DCMG was made but it doesn't study the impact of EVs on it.

Wang et al.[34] and Sayed et al.[35] both proposed great studies but they aren't based on practical data and don't extend their study to a large time interval which loses in exhaustiveness as it doesn't account for seasonal effects.

Finally, combining the 2 models allows the study of a macroscopic DCMG based on practical data which evaluates the impact of EVs and projects a simulation for 2030.

Chapter 3

Methodology and scenarios

This chapter describes the methodology employed and the scenarios implemented as part of this thesis.
The methodology justifies the rationale behind the choice of each scenario and explains its objective while the scenarios are the tool that apply the methodology and enable the various expected results to be highlighted.
Most of the numerical values assigned to the parameters and the justifications for the assumptions on which they are based for the sizing and design of the scenarios are justified in Appendices.

3.1 Methodology

The used methodology provides an independent parametric study of the model. By changing one parameter per scenario, a behavioural study of the DCMG is carried out. The origins of these parameter variations can be socio-cultural or technical. It allows to understand the way the DCMG interacts and the way it's impacted by changes. Comprehending these dynamics facilitates the interpretation of the results and validates the model since its outputs are predictable and common to the conventional studies of power flows on power grids.
The analysis then shifts to evaluating the impact of EVs on the DCMG. Initially, the duality between CC and CP loads is examined. Following this, the effect of integrating EVs is described. Lastly, a simulation of what should be the situation in 2030 due to the policy of Belgium concerning company cars is provided and discussed.

Scenarios are constructed on a flexible architecture where loads, batteries, PVs, and grid connection point can be positioned at various nodes, defining different base cases. Those are then developed from these base cases, with the placement of the EVCS at specific nodes distinguishing each scenario.

3.2 Load profiles

Several load profiles have been generated using different arrivals and departures data. They were obtained thanks to the stochastic model which has been described in section 2.1. The parameters used to simulate them (initial SOC, standard deviation of SOC, characteristics of the vehicles in the fleet,...) are gathered in Appendix A: Stochastic model and are the same for each profile except if it is mentioned.

Weekday

This profile is based on the data of arrival and departure that can be found in the paper upon which the stochastic model is based [19] but it has been resized to fit the figures of the scenarios. Figure 3.1 is displaying it while Figure 3.2 shows the power requirement profile that corresponds to it.

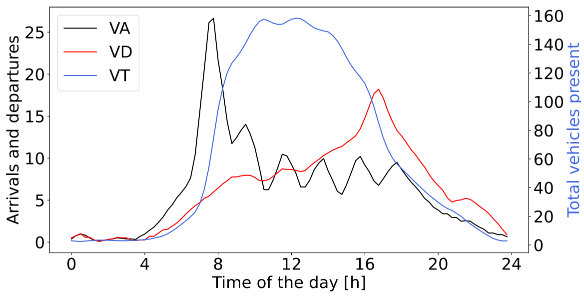

Figure 3.1: Number of arrival (VA), departure (VD) and total number of vehicles present (VT) during a regular workday

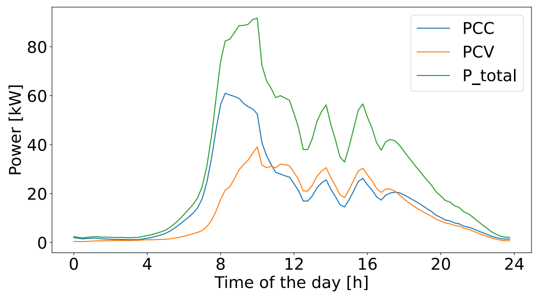

Figure 3.2: Power requirement resulting from the EVs demand of workers during a normal working day

Weekend

These profiles are identical to those shown in 'weekday' but the inputs have been divided by 10. This adjustment is based on the fact that people are less likely to come to business premises during the weekend but some comings and goings can be expected. As a result, the corresponding graphs mirror those presented above, but with a scaling factor of 10.

Punctual workers

In this case, it is assumed that people are punctual, resulting in shorter intervals for arriving at and leaving their offices. The profile is designed such that the total number of vehicles at the EVCS during the peak period matches the 'weekday' profile representing the maximum capacity of the car park.

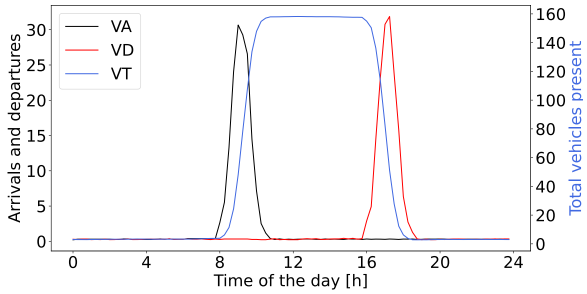

Figure 3.3: Number of arrival (VA), departure (VD) and total number of vehicles present (VT) when workers are punctual

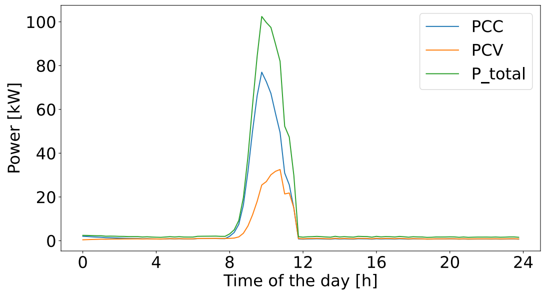

Figure 3.4: Power requirement resulting from the EVs demand when workers are punctual

Global models

Two yearly models are created from these three profiles. In both cases, the five days of the week are exclusively generated from either the "weekday" profile or the "punctual workers" profile. The two weekend days are made from the "weekend" profile. From now on, "Weekday&weekend" and "Punctual&weekend" will respectively refer to these two annual profiles.

It is assumed that every day the initial parameters are set again to what they were at the beginning of the day supposing that workers have access to a charging station at home.

2030 models

These models have been generated to simulate the fleet of vehicles expected at a business premise in Belgium by 2030. Indeed, from this date, company cars are supposed to be only electric vehicles.

Here the two global models are based on the same as those described in "Global models" but the parameters of the vehicle fleet have been changed. Compared to the parameters given in Figure 5.2 which is in the Appendices, only the characteristics relating to the four 100% EVs have been taken which are *the Nissan Leaf, the Toyota RAV4, the Mini E Cooper and the Tesla Roadster*. Moreover, the parameter K, representing the penetration level, has been increased to 100% instead of 25%.

Since the arrivals and departures haven't been changed, the plots are the same as those in "Weekday" and "Punctual" which respectively correspond to Figure 3.1 and Figure 3.3. However, the figures for the resulting power requirements are described in Figure 3.5 and Figure 3.6 for "Weekday 2030" and "Punctual 2030". In the same way that it has been done before, "Weekend 2030" mirrors "Weekday 2030" but with a factor of 10.

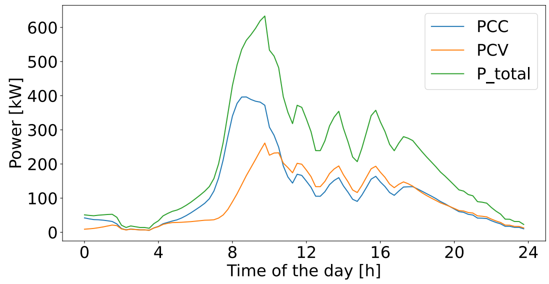

Figure 3.5: Power requirement resulting from the EVs demand of workers during a normal working day in 2030

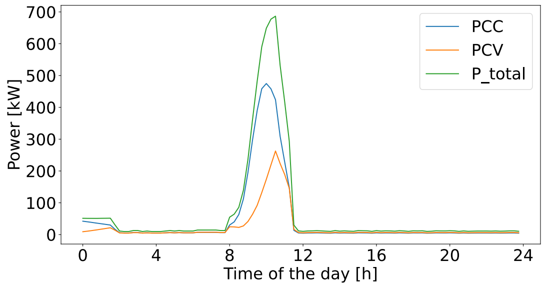

Figure 3.6: Power requirement resulting from the EVs demand when workers are punctual in 2030

3.3 Scenarios

This section describes the base cases on which scenarios are based. They are relatively simple DCMG architectures where the EVCS hasn't been added yet.
The systems include an industrial load behaving as a constant power load which has been provided by the teaching staff and which is described in Appendix B : Scenarios. There are also non-dispatchable DG units represented by 750 PVs which produce a negative constant power load as explained in section 2.2. A dispatchable DG unit is represented by a battery of $600kWh$ which has a (dis-)charge rate of $150kW$ and is initialized with a SOC of 20%. A point of connection (POC) with the main electric grid is always present.

The reference voltage of the MG in the various architectures is always set at $700V$ and the cross-section of the lines is $120\,mm^2$. The corresponding line resistance is $0.153\Omega/km$ [36].
The main features of the different sources of production and consumption are gathered in Table 3.1. Information about the load models is also detailed in it. The total energy provided in the table is computed over a full calendar year. The "W&w" and the "P&w" refer respectively to "Weekday&weekend" and "Punctual&weekend".

	Industrial load	PV	W&w	P&w	W&w 2030	P&w 2030
Max power [kW]	70	200	91.6	102.4	616.5	640.9
Min power [kW]	12	0	0.2	0.19	1.2	1
Mean power [kW]	35.9	29	23.1	8.2	137.3	48.6
Total energy [MWh]	315	254	202	72	1202.5	426

Table 3.1: Loads and generation units characteristics

The scenarios are presented after the base cases on which they rely. They consist of

the addition of EVCS at various locations on the DCMG to study the impact of adding EVs considering different base cases.
Scenarios are labeled such that the letter refers to the base case upon which they are based and the number indicates the specific scenario within that base case. Line lengths are specified in meters between the lines connecting two nodes on the base case and scenario representations.

Base case A

This base case is made up of three nodes and a POC to the grid. The office building represented by the industrial load is assigned to node 'a' and the PVs as well as the battery have been put at node 'c'. It is represented in Figure 3.7.

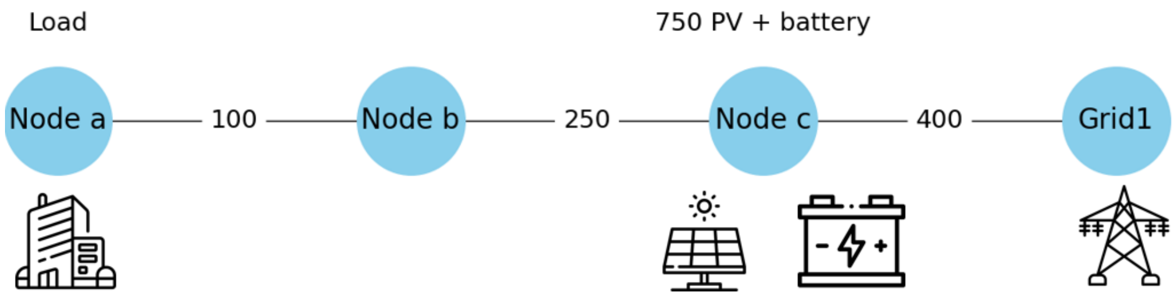

Figure 3.7: Base case A of the DCMG

Scenario A.1

The way this scenario is designed may seem naive because of the under-use of node 'a' and node 'b' knowing the solar potential there is on the roof of the building of the industrial load and the roof of the parking area. However, this approach offers the advantage of isolating all the different kinds of loads such that their behaviour can be independently studied.

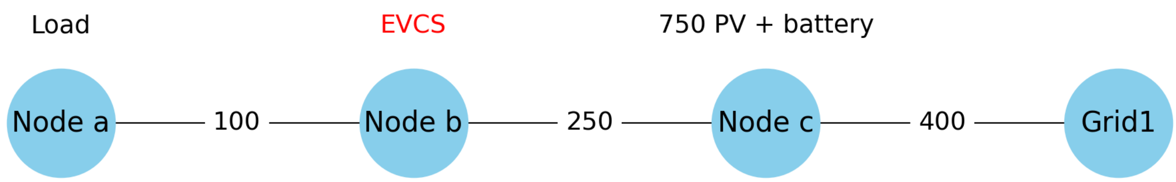

Figure 3.8: Scenario A.1

Base case B

This base case consists of three nodes and one POC. The load, the battery and a part of PVs are assigned to node 'a'. The rest of the PVs are placed at node 'c'.

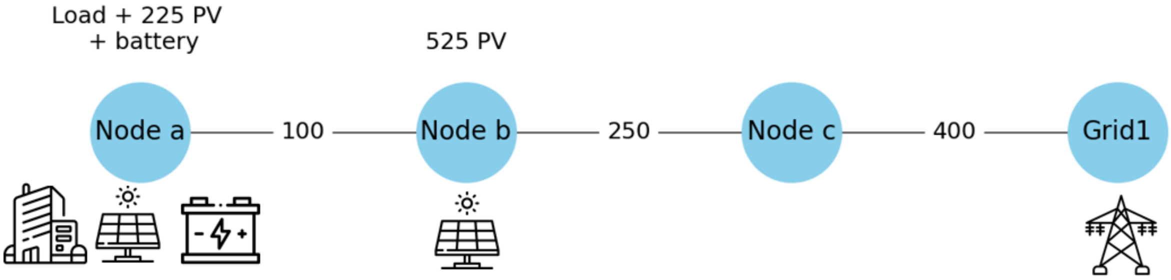

Figure 3.9: Base case B

Scenario B.1

This scenario is realistic given the justification of the assumptions that have been made in Appendix B : Scenarios and the appropriate placement of the PVs. It is also practical to locate the car park closer to the office building.

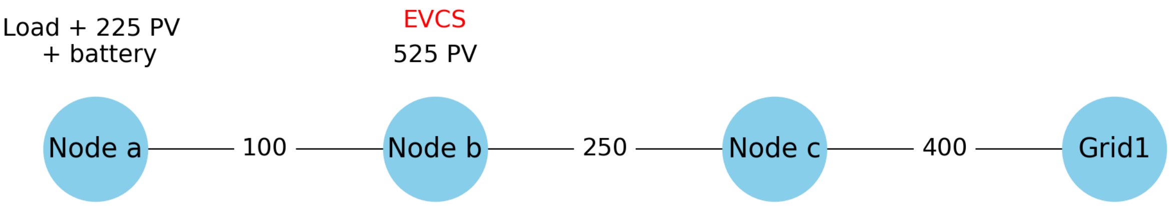

Figure 3.10: Scenario B.1

Base case C

Base case C is constituted of four nodes and one POC. Node 'a' is composed of the load and a part of the PVs while node 'b' has the rest of it and node 'c' has the battery. Scenarios based on the base case C include an additional node, providing more flexibility and enabling the splitting of the EVCS.

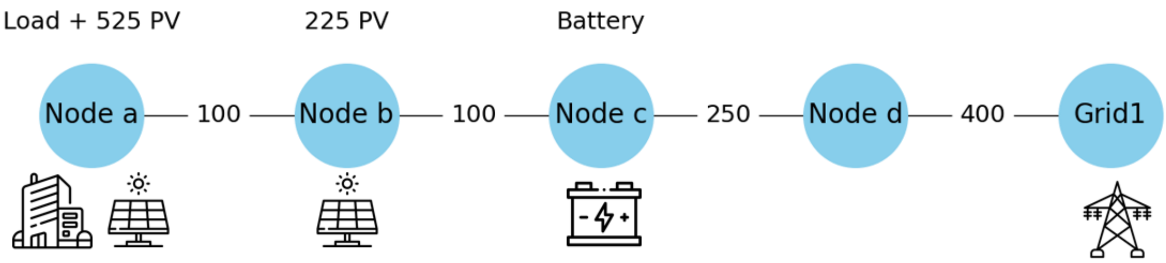

Figure 3.11: Base case C of the DCMG

Scenario C.1

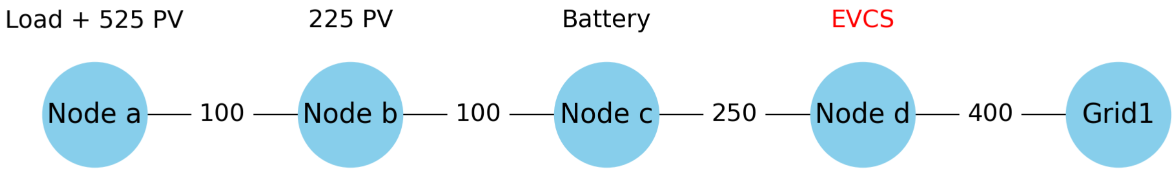

Figure 3.12: Scenario C.1

Scenario C.2

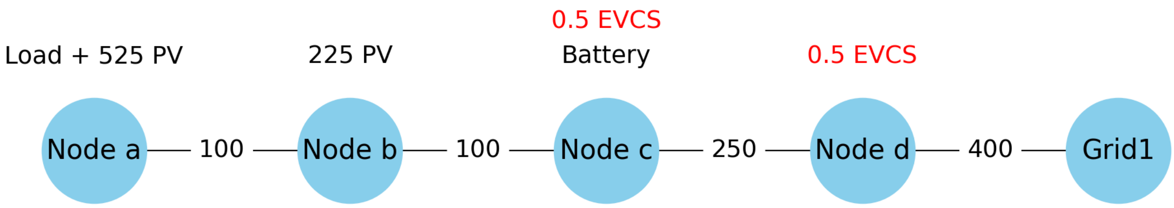

Figure 3.13: Scenario C.2

Scenario C.3

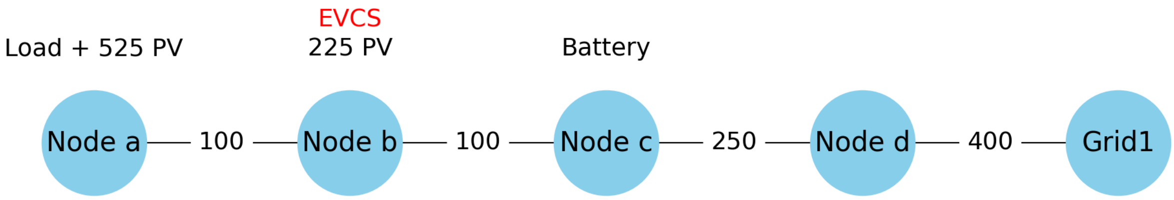

Figure 3.14: Scenario C.3

Base case D

This last base case contains six nodes and one POC which has the particularity of being in the middle of the DCMG. The normal composition of the system has been divided in two and put to each side from the POC. The detailed architecture is described in Figure 3.15.

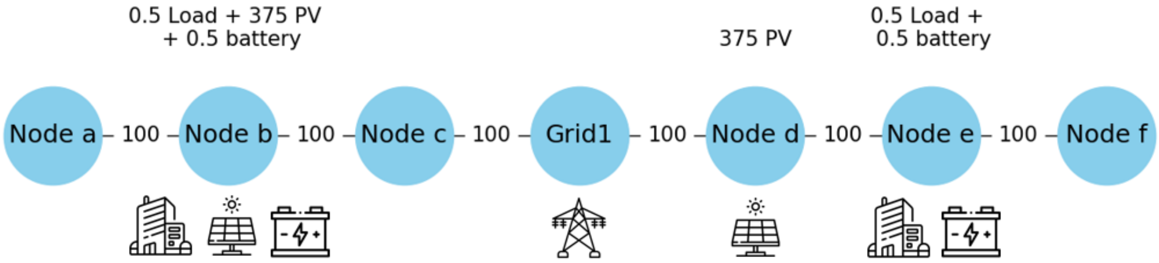

Figure 3.15: Base case D of the DCMG

Scenario D.1

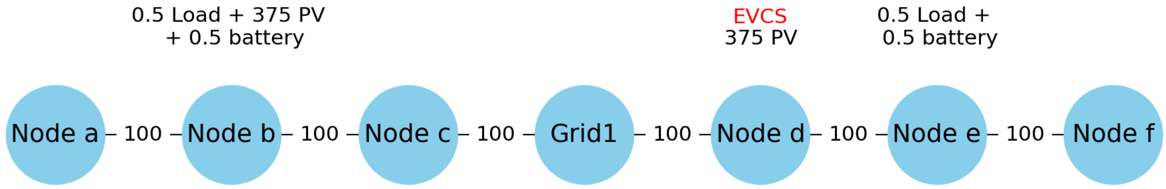

Figure 3.16: Scenario D.1

Scenario D.2

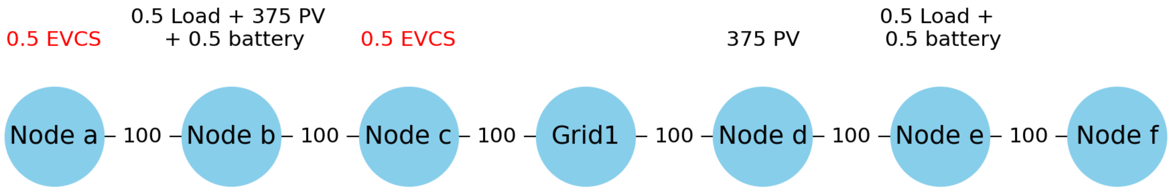

Figure 3.17: Scenario D.2

Scenario D.3

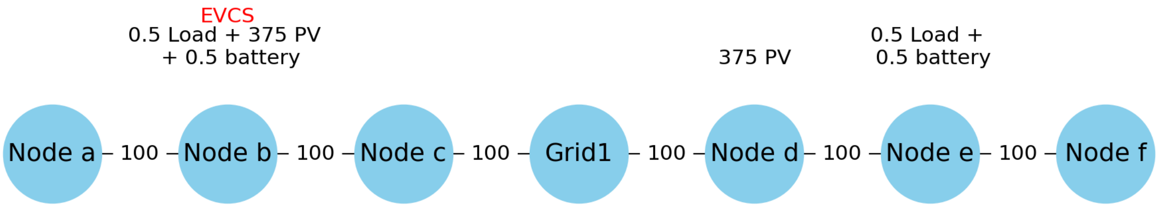

Figure 3.18: Scenario D.3

Scenario D.4

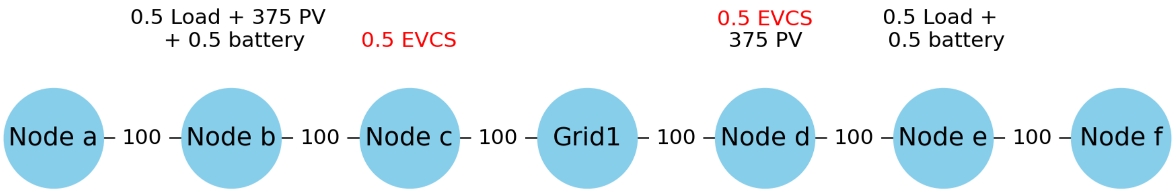

Figure 3.19: Scenario D.4

Scenario D.5

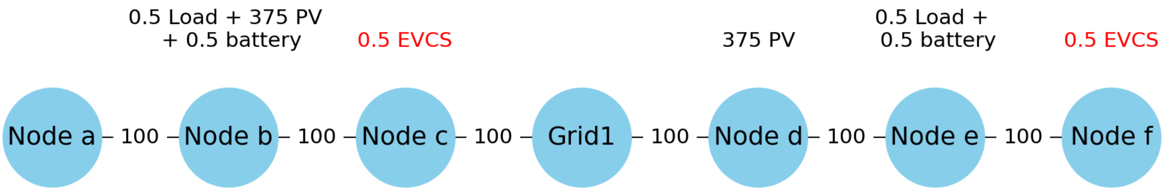

Figure 3.20: Scenario D.5

Scenarios for 2030

The scenarios for this forecast of the 2030 situation are based on scenario B.1 which is a simple and realistic scenario. It is using the 2030 load profiles for the EVCS. It includes two cases:

"The unmodified case" uses the existing B.1 configuration with 2030 load profiles for the EVCS, allowing the impact of future company car policy to be assessed on an existing system that has not been adapted to accommodate this increased fleet of vehicles.

"The adapted case" which has the same architecture as the B.1 scenario but the production and storage units have been scaled up to ensure the DCMG performs properly when the EVCS is added. The target was to achieve a SCI and a SSI above 50% which is an arbitrarily chosen value but which is a reasonable goal for a well-operating DCMG. The production site was sized to balance the energy sent to and required from the grid and maintain voltage stability between 0.95 pu and 1.05 pu.

To do so, the new sizing is based on the previous scenarios and is scaled to meet the increase in demand. As shown in Table 3.1, there is roughly a factor 6 for the maximum power and the total energy between the "Weekday&weekend" and the "Weekday&weekend 2030" load profiles.
Consequently, the number of PVs has been multiplied by six, resulting in 4500 PVs. The battery capacity has also been increased to 1000 MWh, allowing it to supply power for approximately 6 hours at the mean consumption level. Its increase has not been as great as the number of PVs because night-time consumption has not increased much as electric vehicles are mainly in the car park during working hours.

3.4 Constant current vs constant power load

The scenarios outlined in this section aim to highlight the differences between CC and CP loads. To study each aspect of their behaviour independently and understand their impact on a global model, the scenarios have been divided into several parts. The methodology applied to each scenario is always the same: all loads on the DCMG are set as CC loads and compared to the situation where all loads are set as CP loads.
As mentioned in section 2.2 and highlighted by Equation 2.21, the power absorbed by a CP load remains unaffected by the node voltage, for a CC load, it varies proportionally with the node voltage. To observe the impact it has on the DCMG, each scenario is composed of an overvoltage and an undervoltage situation where the mean voltage on the MG is either above or below the reference voltage due to unbalance of consumption and production.
All scenarios are based on scenario A.1 with the "Weekday&weekend" load profile for the EVCS. The only difference is the number of PVs. To create the load unbalances, the under voltage situations are simulated with 500 PVs while the overvoltage cases are simulated with 5000 PVs.

First, scenarios with constant production and constant consumption were generated. To achieve this, both production and consumption were set to the mean power values shown in Table 3.1.
The same scenarios were then implemented with the only difference that a battery was added. In the case of overproduction, the battery was initialized with a SOC of 20% such that it can charge for a certain amount of time. On the other hand, for the overconsumption scenario, the storage was put at a SOC of 95% to allow it to discharge for a certain period. To complete the study of this case, a simple variation of + 2 kW and - 2 kW in the industrial load was also implemented in other scenarios.
A global model was finally studied.

Chapter 4

Presentation and discussion of the simulation results

This chapter presents the simulation results obtained from the scenarios described in chapter 3 and discusses the conclusions that can be drawn from them.
The notion of "better performing" DCMG will be used on multiple occasions in the following sections but it is first imperative to establish a clear definition of what constitutes a well-operating DCMG. Defining "better" requires a rational comparison, ensuring that both scenarios achieve the same objectives.
What defines a better DCMG ? Is a more energy-efficient or independent MG preferable? What is the definition of independence ? Is it best defined by power exchange or the number of interactions with the main grid ? Is it better if the MG provides more power than it requires or the reverse ?
Those questions don't have unanimous responses as the optimal solution depends on the context. Power balance on an electric grid is instantaneous because electricity is hard to store. Depending on the time the main grid might benefit from help from the MG, either providing or requiring some power from it, while at other times, it may not. Even if the system is well designed and appropriately sized as the DCMG is mainly dependent on RES, depending on the year, the season, and the day, it could not be suited for certain times.
Despite the complexity of providing a single universally applicable definition, this thesis bases its definition of a well-performing DCMG on two key aspects: stability and independence.
It means that the optimal DCMG is characterized by minimal voltage deviation, with extreme values kept as close as possible to 1 pu and the lowest number of interactions and energy exchanges with the main grid.

The variables that are studied are the voltage, the self-consumption and self-sufficiency index, (SCI) and (SSI) respectively, the current, the power, the energy required from and sent to the main grid and the line losses. The results can take the form of numerical values or plots. Numerical values are always referring to mean values except if it's specified. In the tables, the 'E.' stands for energy.

The SCI and SSI are important metrics used to assess the performance and sustainability of renewable energy systems.
The SCI represents the proportion of energy consumed directly from renewable sources compared to the total energy produced by the renewable energy system. A higher SCI indicates greater self-consumption of renewable energy produced on-site, which is generally desirable as it reduces dependence on grid energy and increases energy independence. Mathematically, SCI is calculated as the ratio of the self-consumed energy to the total generated energy and is expressed as follows:

$$SCI = \frac{Consumption}{PV\_prod} = \frac{Load\_total + charge}{PV\_prod} = \frac{CCE + CPE + charge}{PV\_prod} \tag{4.1}$$

where PV_prod is the total energy produced by PVs during the period of interest, $charge$ is the energy absorbed by the batteries and CCE and CPE are respectively the total energy demanded by CC and CP loads.

SSI measures the extent to which a system can meet its energy demand solely from its renewable energy production, without relying on external sources such as the main grid. A higher SSI indicates a greater capacity of the system to meet its energy needs independently which is often a goal for off-grid or remote locations where network connectivity is limited or unreliable. It is calculated as the ratio of energy consumed from RES to the total energy demand of the system and is written as follows :

$$SSI = \frac{Sufficiency}{Load\_total} = \frac{PV\_prod + discharge}{CCE + CPE} \tag{4.2}$$

where $discharge$ is the energy provided by the batteries on the grid.

Python is the only programming language that has been employed to get these results. Except for Excel, which has been used as an intermediate to store data, no other tool was used in this work.

The qualitative results of the behavioural study are discussed first. The numerical results aren't relevant because the scenarios on which they are based have been arbitrarily chosen and they don't directly aim at answering the research questions of this thesis. The goal is to understand how the DCMG reacts. The colours of the arrows in the tables indicate the positive or negative impact of the variation in relation to the definition of a performing MG. Green signifies a positive impact while red means a negative one. This is followed by a study of the comparison between CC and CP loads. Finally, the impact of EVs on the DCMG is described before presenting a forecast of the situation in 2030.

4.1 Behavioural study of the DCMG

As previously said, this section aims to provide a complete understanding of the ways the DCMG reacts to various parameter deviations which can be embodied by socio-cultural changes or technical modifications. Only the trends of the behaviour are analyzed because the figures are based on an arbitrary case and no conclusions can be drawn from them.
The plots have been taken from scenario A.1.

4.1.1 Voltage variation

Voltage is a critical parameter in a DCMG and as for larger electric grids, its stability is essential for the proper operation of the system. Voltage stability is determined by the balance between power generation and consumption. Therefore, fluctuations are caused by imbalances. Voltage is a global variable such that all nodes are closely linked and typically follow the same trend.
In Figure 4.1, the total power required from EVs on the DCMG and the voltage at the mentioned node are plotted for the first day of the year in scenario A.1.

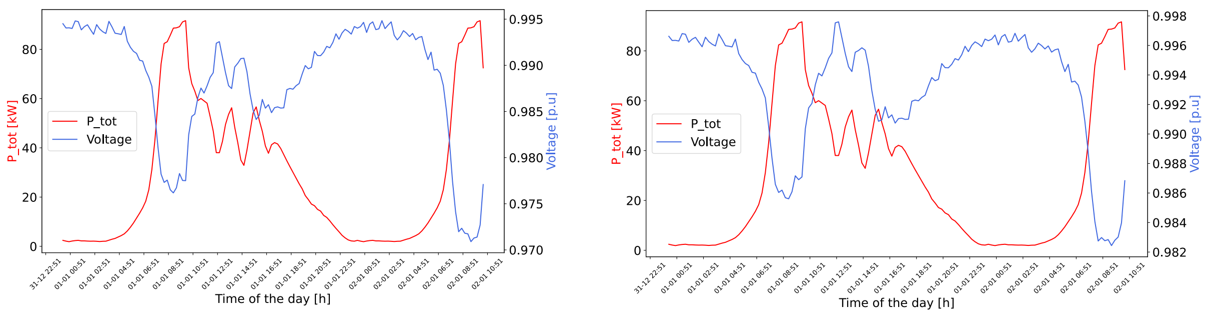

Figure 4.1: Evolution of the voltage in function of the total power requirement from EVCS at node 'b' (left) and node 'c' (right) for scenario A.1

It shows that the voltage is nearly perfectly inversely proportional to the load variation. Although the power requirement from EVs is significant, it is not sufficient for the voltage to perfectly fit the curve because of the influence of the other sources of consumption and production.
It can be noted that despite the EVCS being located at node 'b', both nodes display

similar voltage profiles, highlighting the close link between nodes' voltage which indicates that local variations in load can influence the entire system's voltage profile.
In short, when power consumption increases, the voltage drops and when consumption decreases, the voltage rises, assuming constant power generation. Conversely, when power production increases, the voltage rises and when production decreases, the voltage drops. Everything is a matter of equilibrium.

4.1.2 Current variation

As with voltage, current is also a question of balance but unlike it, current is more a local variable and it is proportional to the load variation. It varies significantly depending on the specific loads or generation sources connected to each node.
In Figure 4.2, the total power required from EVs on the DCMG and the current at the mentioned node are plotted for the first day of the year in scenario A.1.

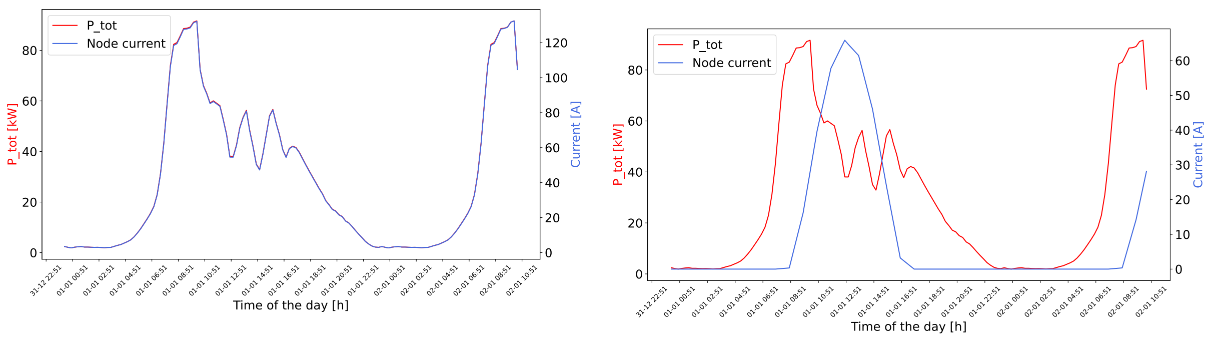

Figure 4.2: Evolution of the current in function of the total power requirement from EVCS at node 'b' (left) and node 'c' (right) for scenario A.1

It can be observed that the plots are completely different. The first plot shows that the current is perfectly proportional to the variation induced by the EVCS which is located on this same node, unlike the current profile at node 'c' where the load profile of the PV production can be distinguished. These differences highlight the localized nature of current variations.
It's important to note that these behaviours were extracted because each node is assigned to a specific load or production source. If several features were placed on the same node, the resulting current would have been the result of all contributions.

4.1.3 Variation of production

The origin of a variation in production is mainly technical since it only involves PVs. Naturally, an increase in production reduces the energy required from the main grid while increasing the energy returned to it.

The SCI drops with the increased PV production, unlike the SSI which rises because the 'sufficiency' increases as it can be inferred from Equation 4.1 and Equation 4.2.
Typically, line losses are expected to increase because of higher current on the lines but it will be discussed in section 4.3 that this is not always the case.
Overall, the opposite can be said for a decrease in production.
Conclusions drawn from an increase or a decrease in production are gathered in the following table. The results discussed below assume a constant consumption level. The upward arrows indicate an increase while the downward ones indicate a decrease.

	SCI	SSI	E. required	E. given	Line losses
Increase of production	↘	↗	↘	↗	↗
Decrease of production	↗	↘	↗	↘	↘

Table 4.1: Impact of production variation on DCMG characteristics

4.1.4 Variation of consumption

The variation in consumption can be due to both socio-cultural and technical changes. Indeed, these variations can take the form of shifting in people's habits such as adopting 100% EV instead of HEV, choosing smaller or larger EVs, installing fast-charging or slow-charging stations, being punctual or arriving within a broad time frame, engaging in car-sharing,...
An increase in consumption necessitates more energy from the main grid while reducing the energy returned to it.
The SCI rises given the increase of consumption, unlike the SSI which drops because the 'sufficiency' remains the same while the total load increases as derived from Equation 4.1 and Equation 4.2.
Line losses are typically increasing because of higher current on the lines but section 4.3 shows that it is not always the case.
Overall, the opposite can be said for a decrease in consumption.
Results are summarized in Table 4.2 and assume a constant production level.

	SCI	SSI	E. required	E. given	Line losses
Increase of load	↗	↘	↗	↘	↗
Decrease of load	↘	↗	↘	↗	↘

Table 4.2: Impact of load variation on DCMG characteristics

4.2 Constant current VS constant power load

The scenarios on which this section is based are separated into several parts to highlight the differences between CC and CP loads. They have been cited in section 3.4. In the following subsections, the scenarios where all loads are set as CC loads or CP loads are often referred to as the 'CC case' or 'CP case' or 'CC simulation' or 'CP simulation' for brevity and clarity.

4.2.1 Constant production and constant consumption

The purpose of these scenarios is to determine if there is any intrinsic difference between the two modes when no variation is detected, with only the voltage on the grid being different in function of the case. The idea behind this case is to observe the difference that is supposed to exist between CC and CP loads. As indicated by Equation 2.21 and Equation 2.22 which are again written here for clarity, the current should be higher for CC loads than CP loads in overvoltage situations when working at the same power. In undervoltage situations, these observations are reversed.

$$PL_i = P_{Pi} + hP_{Ii}V_i + h^2 P_{Ri}V_i^2 \tag{4.3}$$

$$IL_i = \frac{P_{Pi}}{V_i} + hP_{Ii} + h^2 P_{Ri}V_i \tag{4.4}$$

The results will try to confirm that and observe what are the other effects that it could have on the DCMG. The current and power values in the tables refer to the current between node 'b' and node 'c' which is the connection between the node where the PVs are installed and the node where the EVCS is located. This choice was made arbitrarily, as similar observations can be made between node 'a' and node 'b', where node 'a' is the node with the industrial load.
The power values represent maximum values.

Overvoltage

	E. given [MWh]	Line losses [MWh]	Current [A]	Power [kW]
CC	951.72	17.94	117.29	82.69
CP	956.5	17.88	116.49	82.14

Table 4.3: Impact of CC and CP load in overvoltage and constant production and consumption

Table 4.3 shows that in overvoltage situations, CP loads are less demanding than CC loads. Indeed, the line losses, current and power are lower. This allows the MG to inject more power into the main grid as less is consumed directly by it. The energy required from the grid is zero since there is always overproduction on the DCMG and the voltage is globally higher on it. Currents are logically higher when only CC loads are implemented so it increases the line losses following Joule's law [9].

Undervoltage

	E. required [MWh]	Line losses [MWh]	Current [A]	Power [kW]
CC	548.44	9.25	117.29	80.94
CP	559.19	9.57	119.05	82.14

Table 4.4: Impact of CC and CP load in undervoltage and constant production and consumption

The table highlights that CC loads perform better in undervoltage situations compared to CP loads. The reverse observations can be made from Table 4.3. In this case, the energy sent to the grid is zero due to consistent underproduction on the DCMG resulting in a voltage magnitude globally lower than the reference voltage.

Discussion

The intuition provided by the mathematical formula in Equation 2.21 is confirmed. For CP loads, the current and power are higher when the voltage is below the reference value and lower when it is above compared to CC loads.
Moreover, the constant current and constant power properties of CC and CP loads can be observed when comparing the two tables and observing the current and power columns. These properties are not impacted by the amplitude of the voltage. Comparisons for the voltage behaviour in the two cases will be discussed in the following subsection with the help of plots.

4.2.2 Variation of the load

The scenarios implemented in this subsection aim to induce a variation that allows the observation of a difference in consumption or production, creating a variation of power on the grid. This will enable the study of the dynamic response of CC and CP loads to changes. The goal is also to observe if there is an accentuation of the CC or CP behaviour when facing situations closer to or further from the reference voltage.
In the following plots, the differences are computed by subtracting the values obtained in the CC simulation from those in the CP simulation. The plots result from variations observed at node 'c' where the PVs and the battery are installed.

Overvoltage

In this case, the battery is initialized with a low SOC and is charging itself for the first instances of the simulation. The difference between the cases where all loads are put as CC loads versus CP loads is compared both for voltage and current as shown in Figure 4.3.

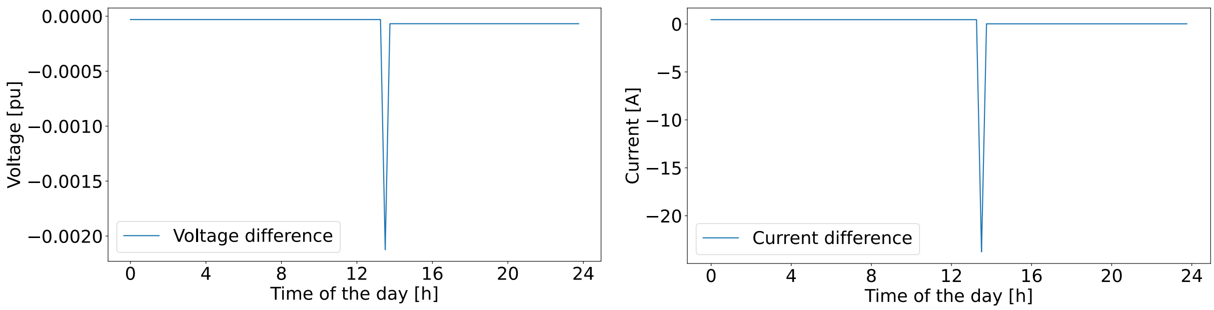

Figure 4.3: Voltage (left) and current difference (right) between CC and CP simulation with a variation induced by a battery

It shows that the stable phases before and after the variation aren't set at the same values, indicating that the deviation from the reference state increases the difference between CC and CP cases.
It also appears that there is a dynamic behaviour difference between CC and CP situations as the difference is temporarily increased at the moment the variation occurs. This behaviour of the DCMG will be further investigated by increasing the consumption of the industrial load, to ensure that the observations aren't solely due to the intrinsic behaviour of the battery.

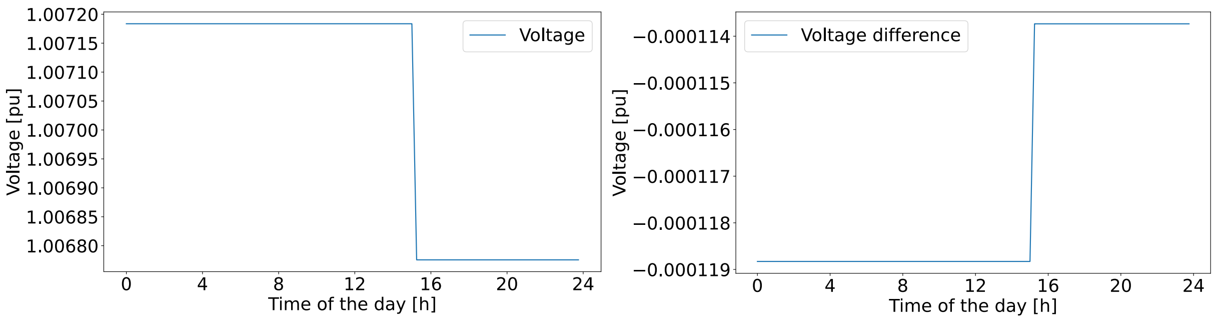

Figure 4.4: CC load voltage (left) and voltage difference (right) between CC and CP simulation with a variation induced by the industrial load in an overvoltage situation

Figure 4.4 and Figure 4.5 are made from observations at node 'a' where the industrial load is located. The voltage and current plots for the CP load are not shown because they are very similar to those for the CC loads, as confirmed by the difference plots, which indicate that the difference is small. It can be seen that both the voltage difference and the current difference decrease when the voltage approaches the reference value.
In overvoltage situations, for the same inputs, the voltage on the DCMG is higher for the CP case but the current is lower. This can be stated because the voltage and

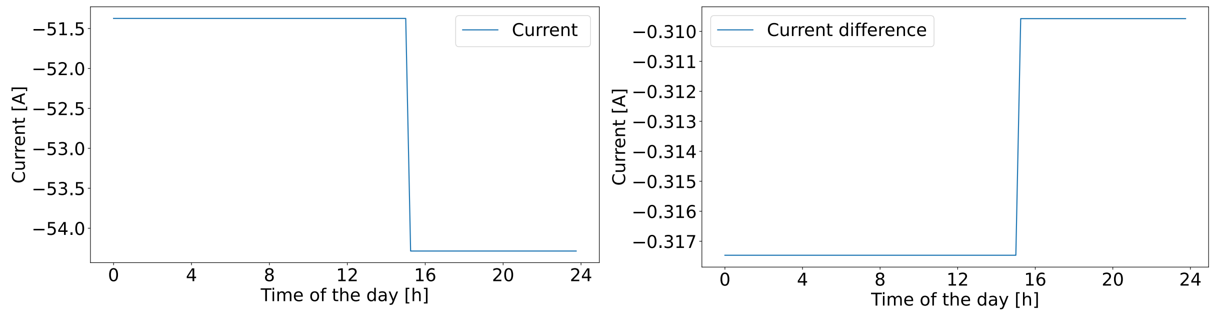

Figure 4.5: CC load current (left) and current difference (right) between CC and CP simulation with a variation induced by the industrial load in an overvoltage situation

current differences are negative, as determined by the sign of the voltage and current. According to the definition provided at the beginning of this subsection, the differences were calculated by subtracting the CP result values from the CC result values.
Most importantly, the plots show no dynamic behaviour difference between the CC and CP simulations. The changes are smooth and follow the differences induced by deviations from the reference state. Therefore, the abnormal behaviour observed earlier is likely due to the intrinsic behaviour of the battery.

Undervoltage

In this case, the battery is initialized with a high SOC and is discharging itself for the first time steps of the simulation. This time, the case where the variation is due to the battery is no longer considered and the situation where the deviation is due to the decreasing of the industrial load is directly studied.
This additional scenario analyses the same characteristics as the overvoltage case and aims to confirm what has been observed.

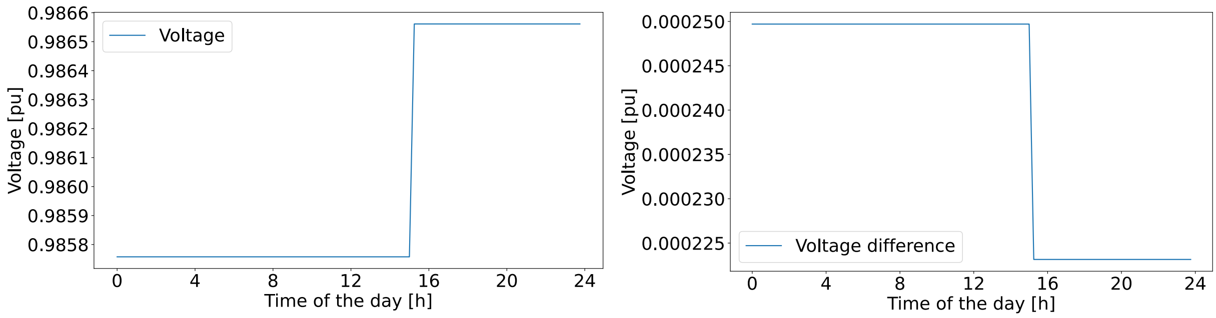

Figure 4.6: CC load voltage (left) and voltage difference (right) between CC and CP simulation with a variation induced by the industrial load in an undervoltage situation

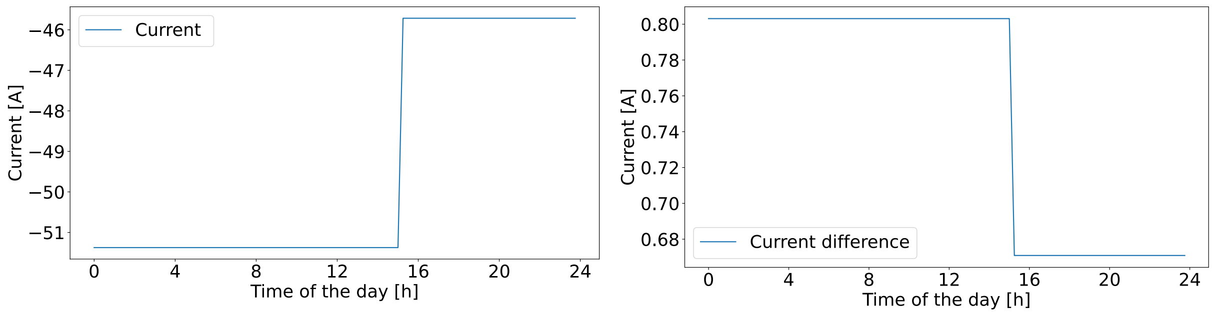

Figure 4.7: CC load current (left) and current difference (right) between CC and CP simulation with a variation induced by the industrial load in an undervoltage situation

The above plots were generated from observations at node 'a' where the industrial load is located. Again, plots for the CP load voltage and current aren't depicted because they are very similar to those for CC loads, as confirmed by the difference plots which indicate minimal differences.
Globally, the same kind of observations can be made but in this case, the system is in an undervoltage situation and the variation of load is a decrease instead of an increase. As explained in section 4.1, the voltage increases following a decrease in consumption and the current decreases accordingly.
The voltage and current differences are smaller as the DCMG approaches equilibrium as for the overvoltage situation. Contrary to the overvoltage situation, here the current and voltage differences are positive meaning that the voltage of the CC case is greater while the current is smaller compared to the CP case.

Discussion

This subsection confirms previous observations and intuitions and provides new conclusions.
The behaviour of the DCMG discussed in section 4.1 has been confirmed. The intuition from Equation 2.21 and Equation 2.22 that the difference between CC and CP simulations is greater when the state of the system is further away from the reference value has been validated. Moreover, no difference in dynamic response behaviour is observed. Regarding the initial impressions influenced by the batteries, the increasing difference between the two cases is not due to different dynamics in their responses. This is because of the stable phase preceding the variation. Indeed, for the overvoltage case, the DCMG with CP loads performs better as explained in subsection 4.2.1 such that the battery charges faster and can stop charging sooner than in the case where only CC loads are implemented. To be precise, it stops at the same time step in both cases but

in the CP case, the battery is almost full such that at the next iteration, it is already able to deliver much more current to the main grid than in the CC case. This explains the voltage and current differences observed. To provide numerical values, the battery gains 1.384% charge with each iteration in the CP simulation, compared with 1.38% in the CC case.

Similarly, for the undervoltage case, the deviation is because the CP case has a poorer efficiency such that the battery is discharging itself quicker inducing a time shift or at least a difference of value at the concerned time step. The battery delivers 0.775% of its SOC at each iteration of the CC simulation compared with 0.791% in the CP case.

In short, no significant difference is induced by variations when comparing CC and CP cases. This confirms the conclusions from the previous subsection regarding the relative performance of CC and CP loads in overvoltage and undervoltage situations.

4.2.3 Global model

The scenarios created for this case aim to validate previous observations and potentially draw new conclusions. The analysis is logically divided into overvoltage and undervoltage situations. However, there are natural times when the voltage is above or below the reference voltage as it is a global model. In this subsection, overvoltage and undervoltage refer to the average voltage of the node being higher or lower than the nominal voltage. Results are presented using global numerical figures gathered into tables. The plots serve illustratively to depict the problem and demonstrate that the mean voltage is higher or lower than the nominal voltage. The voltage plots are based on variations observed at node 'b'. The numerical values in the tables concerning current and power are relative to the line between node 'b' and node 'c'. This approach was chosen for the same reasons mentioned in subsection 4.2.1. The numerical figures for power represent maximum values.

Overvoltage

	E. given [MWh]	E. required [MWh]	Line losses [MWh]	Current [A]	Power [kW]
CC	1127.63	55.34	88.4	84.33	162.94
CP	1136.26	57.86	89.69	83.22	156.52

Table 4.5: Impact of CC and CP loads on a global model with average overvoltage

The same observation as in subsection 4.2.1 can be made. However, what is truly interesting here is that compared to it, the power required from the grid isn't zero. This is because, as explained, the voltage on the DCMG can be under the reference voltage

for a certain portion of time, unlike the scenario of the first subsection where because of the power constant, it was consistently above it.
This new feature shows that more energy is required from the grid in the CP case than in the CC case.

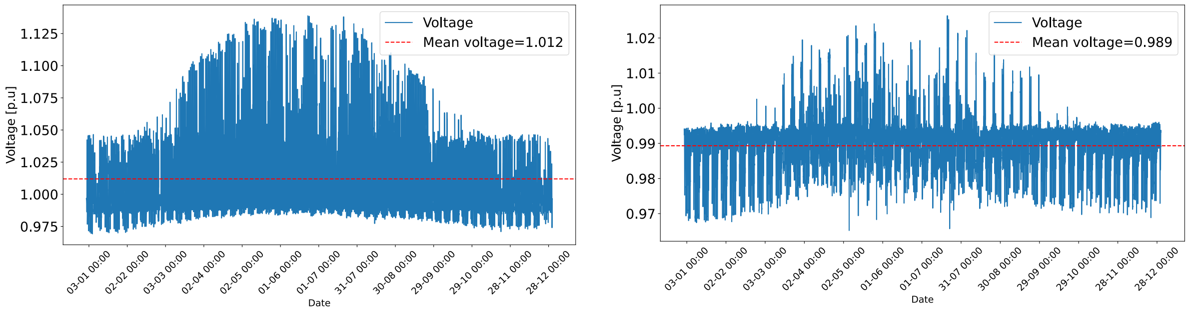

Figure 4.8: Evolution of the voltage on the DCMG for a global model implemented with only CC loads: (left) mean overvoltage and (right) mean undervoltage

Undervoltage

	E. given [MWh]	E. required [MWh]	Line losses [MWh]	Current [A]	Power [kW]
CC	0.49	347.69	6.06	84.33	152.69
CP	0.51	354.36	6.28	85.42	156.52

Table 4.6: Impact of CC and CP loads on a global model with average undervoltage

The same ascertainment can be made for the undervoltage part as well. The property of constant current and constant power for CC and CP loads is again demonstrated by comparing the two tables. It can be observed that more energy is sent to the grid in the CP case than in the CC.

Discussion

This discussion concludes the comparison of CC and CP simulations. The above-explored subsections confirm several features discussed earlier in section 4.1, validate mathematical intuitions, and highlight the similar dynamic responses of the two modes. The observations made on the batteries underscore the conclusions made in section 4.2. In this subsection, where a global model is implemented, both overvoltage and undervoltage situations occur within the same simulation. This provides information about both the energy required from and sent to the grid which confirms the difference in performance between CC and CP simulations depending on the operating voltage.

Line losses are generally higher in any situation for the CP case, suggesting less energy efficiency but when it's in the overvoltage situation it's able to do the same work as the CC case while providing more energy to the main grid. On the other hand, in the undervoltage situation, the CC simulation achieves the targets while asking for less support from the main grid.

Relative to the definition of a well-operating DCMG and the two key aspects linked to it, having primarily CC loads appears to be the best approach. In CC simulations, the voltage is lower than in CP simulations during overvoltage situations, making the system closer to the reference state and resulting in lower power. Additionally, even if the energy sent to the grid is lower, which may seem less efficient, it also means less interaction with the main grid.
In undervoltage situations, the voltage is higher in the CC case, bringing the system closer to equilibrium. It requires less energy from the grid, making it more efficient and most importantly, less dependent on it.

Moreover, Singh et al.[37] discussed the nonlinear behavior of CP loads which complicates control efforts. Their negative incremental impedance can cause imbalances at the load point, decreasing the system's overall damping. This reduction in damping also lowers the system's effective resistance, leading to diminished stability margins and making the system more prone to instability.

In conclusion, both the grid operator and the vehicle owner should avoid having the vehicle too highly charged. Overcharging can damage the battery, as discussed in chapter 1, and the BS EN 61851-23:2014 criterion [20] states that vehicles are in CC mode below 80% of charge. Therefore, to maintain a more independent, balanced system with fewer voltage deviations, it is beneficial for grid operators to keep vehicles below this threshold. The impact of EVs is significant, as their arrival at the EVCS increases the share of CC loads. Without EVs, other loads are mainly CP loads, so EVs contribute to the stability and independence of the system as long as they stay below a certain SOC compared to other loads.

4.3 Impact of EVs

This section investigates the effects of incorporating EVCS into an existing DCMG. The analysis focuses on variables directly related to the two key aspects of the definition of "better" that were introduced at the beginning of this chapter.
The number of interactions between the DCMG and the main grid is evaluated to assess the system's independence while the examination of extreme voltages provides insights into the stability of the DCMG.
Critical variables, such as the maximum current, are also analyzed because of their implications for the DCMG's limitations and the determination of cable cross-sections.

The scenarios are not treated one by one but are gathered in the same plots to highlight general trends as well as exceptions and unique behaviours. To do this, all the results are compared or normalized against the base case to which they refer. The values are expressed as percentages, with 100% indicating the figure observed for the base case. Values below 100% mean a reduction while values above 100% refer to an increase relative to the reference scenario.

Given that adding EVCS is equivalent to increasing the overall consumption on the DCMG, similar conclusions to those presented in section 4.1 can be drawn for the SCI, the SSI, and the energy exchanged with the grid. However, some nuances regarding line losses are discussed in the following subsections.
In the following plots, the circles represent the scenarios with the "Weekday&weekend" load profile simulated at the EVCS while the crosses refer to the "Punctual&weekend" load profile.

4.3.1 Maximum current

Figure 4.9 describes the maximum current observed for each line in various scenarios compared to the maximum value obtained for those same lines in the base case.
The maximum current is a critical parameter to analyze as it directly influences the line cross-section which is mathematically formulated as follows [38]:

$$S = \frac{2\rho I L}{U'} \tag{4.5}$$

where L is the length of the line, I is the current (with the maximum current used here to determine the critical case requiring the highest cross-section) L is the line cross-section and U' is the relative voltage deviation.

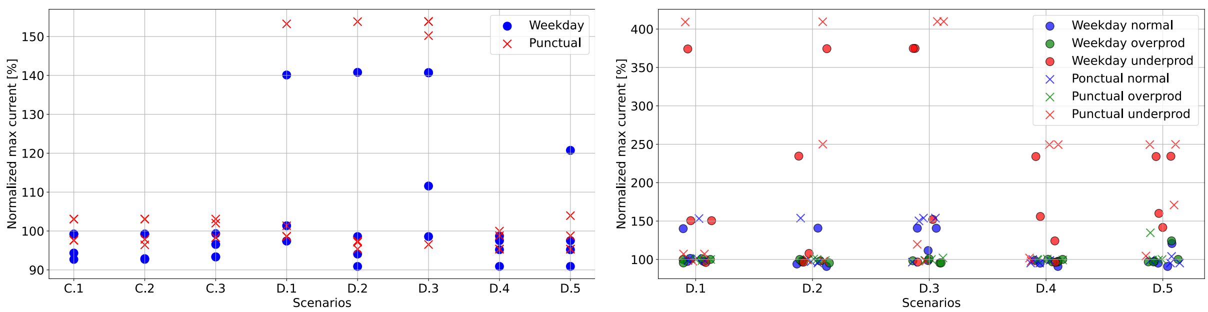

Figure 4.9: Normalized maximum current compared to the base case for each scenario and each cable in normal, underproduction (left) and overproduction (right)

It can be seen from the figure on the left that the maximum currents of the scenarios are generally lower than those of the base case because the maximum currents are determined by the moments of PV overproduction and the addition of EVCS reduces this peak power because the load profiles of the EVs almost coincide with the peak hours of PV production. However, it remains close to the value obtained in the base case because the maxima are defined at weekends when the demand is low due to the lower presence of EVs while PV production remains the same as during the week and as in the base case.

The values for which the maximum current slightly exceeds that of the base case are generally due to the fact that the addition of the EVCS reduces the average voltage of the DCMG such that a slightly higher current is required to transport the same amount of power. This increase is not significant and the figures obtained still result from overproduction rather than load demand.

On the other hand, there are cases where the maximum current is significantly higher than in the base case. This occurs on lines directly affected by the addition of the EVCS and when the parking is not strategically placed. It results in the accumulation of the power needed for industrial loads and the power required for EVs. This leads to scenarios where the demand exceeds peak production such that the maximum currents are determined by the consumption peak.

The plot on the right supports those observations since the results for the overproduction and the underproduction cases have been added. It shows that in overproduction scenarios, the maximum current is less likely to exceed the base case maximum. Conversely, in underproduction scenarios, it more frequently exceeds and reaches higher values.
This is because in overproduction cases, the maximum current is strongly fixed by the peak production, whereas in undersized production systems, high-demand situations are more likely to result in power requirements exceeding production.
Finally, it shows that the most problematic scenarios involve the "Punctual&weekend" load profile due to its higher peak power compared to the "Weekday&weekend" profile.

4.3.2 Line losses

Line losses can provide insights into the equilibrium of current distribution within the DCMG and are depicted in Figure 4.10 where each scenario is compared to its base case. The plot on the left offers greater precision due to its smaller scale while the plot on the right illustrates the significant differences in line losses depending on the DCMG's configuration.

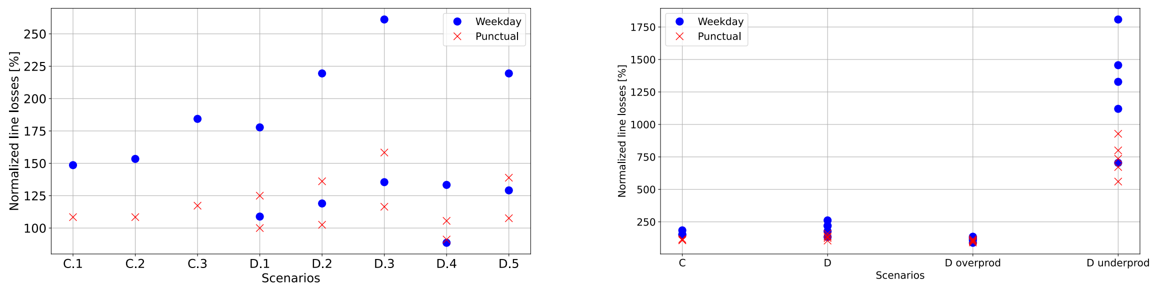

Figure 4.10: Normalized line losses compared to the base case for each scenario and each cable (left) and situation of overproduction and underproduction (right)

These figures confirm that line losses always increase but that some configurations are more favourable than others. Indeed, it shows that despite having the same base case, the location of the EVCS has a significant impact on the line losses. In particular, the overvoltage situation in scenario D.4 shows lower line losses. This can be explained by the strategic placement of the loads on both sides of the POC and by the fact that the EVCS are close to the production sites. This reduces the current transported from the production sites to the POC when it needs to inject current into the main grid, thereby lowering line losses.

Conversely, the figure on the right shows that undervoltage situations are highly unfavorable. As highlighted in subsection 4.3.1, the currents carried on the lines are higher in these cases, not only for peak current but also for the average current. This is due to the increased load which requires more power to be transported from the POC to the additional loads.

4.3.3 Voltage

Voltage is the most relevant variable to analyze when talking about the stability of a DC grid. This explains the choice of showing Figure 4.11 which describes the comparison between the minimum voltage and the maximum voltage reached on the DCMG with the values obtained for the base cases and each scenario.

These figures show that the impact of EVCS on the voltage is relatively small as small percentage values can be observed. As expected, the maximum values as well as the minimum values tend to decrease compared to the base cases due to the addition of the EVCS.
However, it should be noted that this is not always the case as shown by the overproduction and underproduction scenarios. These particular results are due to the position of the POC because it is centrally located and the EVCS are not added symmetrically which disturbs the balance of the system. Moreover, the addition of EVs, which can

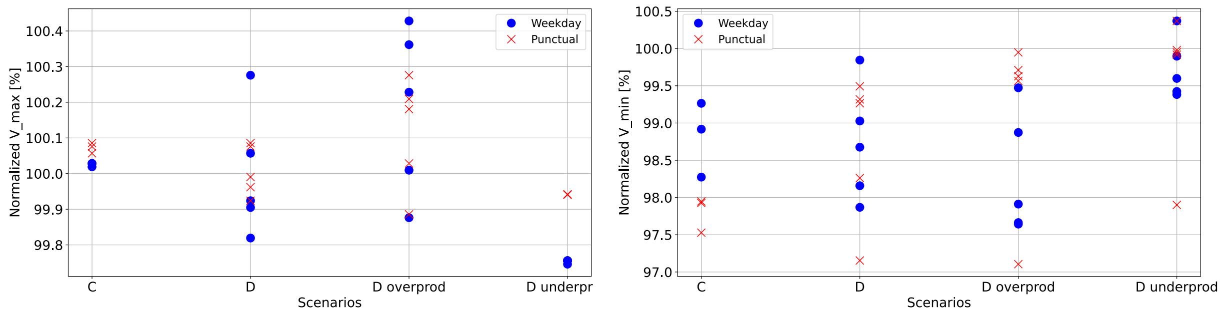

Figure 4.11: Comparison of the maximum (left) and minimum (right) voltage reached on the DCMG for the different scenarios

behave as either CC loads or CP loads, can favour either undervoltage or overvoltage situations as highlighted in section 3.4. This imbalance favours the side of the MG without the EVCS such that a slightly higher voltage is observed on that side.

4.3.4 Interactions

The independence is a key figure of every MG. It can be evaluated by the amount of power exchanged between the main grid and the MG as well as by the number of interactions that occur between them.

Figure 4.12 illustrates the number of power imports and exports between those two systems for the scenarios while highlighting the baseline value when no EVCS are yet added.

The maximum number of interactions is 35040 which is the number of timesteps in the simulation and the number of quarter hours in a year.

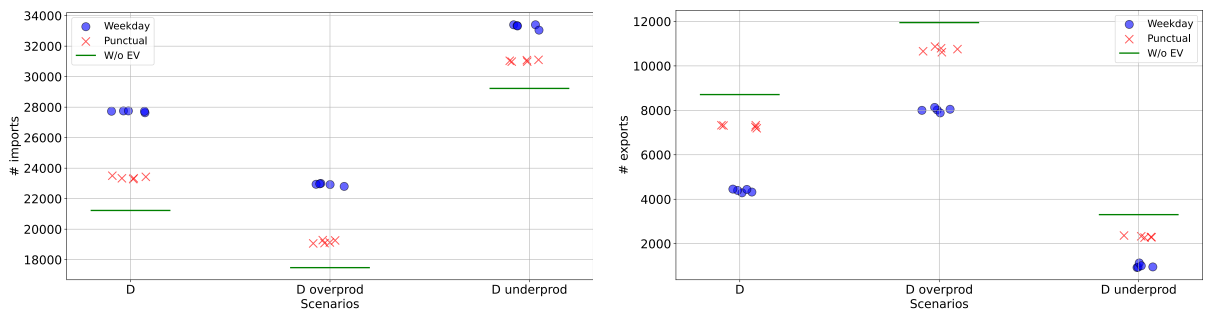

Figure 4.12: Comparison of the number of power imports (left) and exports (right) with the main grid between the scenarios and the base D

The plot shows that the addition of EVs always increases the number of importations conversely to the number of exportations which decreases. When doing the summation of the two figures, it appears that the global number of interactions with the grid increases with the addition of EVCS. The values are more extreme for the scenarios

where the "Weekday&weekend" load profile is used for the EVCS rather than the "Punctual&weekend" profile. This is because, despite the higher peak consumption of the latter profile, the former has a higher overall energy consumption, which drives the number of exchanges.
The plot also underscores that regardless of the scenario, the number of exchanges remains relatively close. For overproduction scenarios, the number of imports decreases whereas for underproduction scenarios, the number of imports increases compared to the normal case. Conversely, the number of exports shows the opposite trend.

4.3.5 Discussion

This section allows to draw additional conclusions regarding the impact of EVs compared to the analysis presented in section 4.1. The results offer further insights into the definition of an efficient MG and its limitations.
The results indicate that the stability of the MG remains relatively unchanged. Although the mean voltage is lower, the maximum and minimum voltages remain close to the values observed before the addition of the EVCS.
However, the independence of the DCMG deteriorates since the number of interactions with the main grid increases. Even though the energy sent to or required from the grid are relevant figures to study, these results can vary significantly depending on the base case and the way the EVCS is integrated. This makes the results inconsistent to analyze. Moreover, different impacts can be observed. For instance, in a system with overproduction, the addition of charging stations could be beneficial by balancing the energy exchange between the MG and the main grid. Conversely, in a system already suffering from underproduction, adding EVs exacerbates the existing issues.

The line cross-section is the only element that imposes limitations on the MG that has been analyzed but other features like transformers, converters, etc can also determine its size. As written in Equation 4.5, line cross-section is proportional to the current. Given that the other parameters remain fixed in this study, the current is the only variable analyzed. It appears that in some cases, the addition of EVCS can benefit the MG by decreasing the peak values that define the cross-section while in other cases the inverse can be observed. The most stressful cases can reach significantly higher values compared to the base case. However, not all lines in the DCMG have the same length, so the impact may be moderated if it affects shorter lines.

The analysis of line losses and maximum current underscores the difficulty of drawing unanimous conclusions on the precise impact of EVs on a DCMG. Although general trends can be observed, exceptions can occur and these trends can extend to extreme values. The impact is highly dependent on the architecture of the MG, the location and distribution of the EVCS, its relative position to other sources of consumption and production and the original balance of the MG before adding the EVs. These factors make it a complex system to analyze where it is difficult to isolate the impact of a single load and to accurately forecast the results.

This section demonstrates that if well-managed, the addition of EVCS can be beneficial but if it is not the case, it can have detrimental effects. Regarding limitations, in most cases, adding EVs increases the stress on the DCMG because of extremer values such as the maximum current. Nevertheless, with smart design, the addition of EVCS can help to mitigate these limitations.

4.4 Forecast for 2030

This section aims to provide an overview of the anticipated situation in a parking lot of a business premise in 2030. It has been based on the most realistic scenario which is scenario B.1.
The scenarios of the case where no changes were made to adapt an existing DCMG and the case where adaptations were made, described in chapter 3, were analyzed separately. The results are presented as numerical figures that have been gathered into tables, displaying the main characteristics obtained for the base case, the cases with the "Weekday&weekend" load profile and the "Punctual&weekend" load profile simulated at the EVCS.

Current existing DCMG

Table 4.7 contains results derived from simulations of scenario B.1 with the 2030 load profiles.

	SCI	SSI	E. given [MWh]	E. req. [MWh]	I_{max} [A]	V_{max} [pu]	V_{min} [pu]
W/o EV	0.804	0.649	48.49	11.56	235.5	1.05	0.98
Weekday	0.991	0.166	2.19	1298.76	1017.83	1.05	0.85
Punctual	0.98	0.336	4.86	501.53	1039.24	1.05	0.85

Table 4.7: Characteristics of the DCMG for 2030 scenarios with no modification to the current existing system

It can be seen above that compared to the base case, all characteristics are drastically influenced by the addition of EVCS. The SCI and SSI are imbalanced highlighting the poor operation of the DCMG as well as the important energy required from the main grid. The voltage reaches critically low points which are not viable for an electric grid. The punctual case is less problematic except in terms of maximum current but these remain significantly high in both cases resulting in a requirement for greater line

cross-section.
About the limitations for the base case, a minimum cross-section of 120 mm^2 was imposed by the maximum current as it was the case for previous scenarios. Regarding the forecast for 2030, a minimum cross-section of 535.83 mm^2 and 546.5 mm^2 is required respectively for the "Weekday&weekend" and the "Punctual&weekend" load profiles. As mentioned in chapter 3, only specific line cross-section sizes are available, and the closest standard size that meets the requirement is 1000 mm^2.

Adapted DCMG

In this scenario, the base case has been modified to accommodate the significant addition of EVCS.

	SCI	SSI	E. given [MWh]	E. req. [MWh]	I_{max} [A]	V_{max} [pu]	V_{min} [pu]
W/o EV	0.2	0.99	1233.91	3.14	1681.99	1.05	0.99
Weekday	0.642	0.66	552.86	514.91	1631.08	1.05	0.95
Punctual	0.402	0.847	922.62	112.48	1665.95	1.05	0.95

Table 4.8: Characteristics of the DCMG for 2030 scenarios with adaptations to meet future demand

The production in the base case without EV is oversized resulting in an unbalance between SCI and SSI and the energy given to and required from the main grid.
It can be observed that the objectives are reached for the scenarios where EVs are added. The SCI and SSI fall within a reasonable interval which is above 50%. Moreover, the equilibrium is nearly perfect between the energy given to and required from the main grid, at least for the "Weekday&weekend" load profile. Both the scenarios where EVs are added respect the voltage limitations by maintaining it between 0.95 and 1.05 pu. To meet these objectives, an oversizing of the production was necessary, leading to overproduction during the summer months. This can be seen by the fact that the maximum current is determined by moments when the DCMG is exporting power to the main grid. These production peaks reach approximately 1600 A compared to the 1000 A necessary for the peak demand as highlighted in the table of the case where no modifications were made.
Concerning the line cross-sections, all scenarios require a cross-section of approximately 850 mm^2 which is also satisfied by the 1000 mm^2 design of the cross-section.

Discussion

The first table underscores the extreme values reached by the SCI and the SSI, the imbalance between the energy required from and sent to the main grid and the minimum voltage which prove the inability of the current existing systems to meet the requirements of 2030. The additional stress placed on the MG can't be adequately managed by the storage and generation units to maintain grid stability within acceptable limits. Moreover, the required increase in line cross-section is nearly multiplied by 10. The utility of MG is not clear anymore when considering the extensive power exchange with the main grid.

The demand for PV systems in a feasible scenario necessitates an unrealistic amount of area, approximately six times the available surface typically found on a business premise, including both the industrial building roof and the parking structure for EVs. The required line cross-section reaching 1000 mm^2 is impractical for low-voltage grids. Furthermore, to achieve reasonable operation of the DCMG, it requires oversizing the production which leads to peak power during sunny periods that is approximately 60% above the peak demand.

A potential solution could involve increasing the reference voltage to mitigate some of these issues. The voltage is inversely proportional to the line cross-section as mentioned in Equation 4.5 and the current decreases linearly when working at constant power as derived from Joule's law [9]. The voltage is therefore having a quadratic impact on the determination of the line cross-section. However, increasing voltage presents its own set of challenges and complications that require changes and investments in the DCMG.

Finally, this case is realistic but it may not be the most optimized for the addition of EVCS, but it also does not represent the worst-case scenario. In other cases, greater or smaller instability or line cross-section limitations could have been observed.
In any case, the conclusion remains consistent, the current MGs are not suited to welcome all future company cars and significant changes and improvements are necessary for optimal operation but it may not be entirely realistic to achieve.

Chapter 5

Conclusion

This thesis contextualizes the evolving role of microgrids in addressing the challenges posed by climate change and the urgent need for decarbonization. RES are decisive in this transition but their intermittent nature and the electrification of transportation have introduced additional stresses on the electrical grid.
Innovative decentralized and distributed solutions needed to be implemented. In this context, microgrids, and especially DC microgrids, offer a promising answer due to their compatibility with PV systems and electric vehicles as they are all fed in DC. These interesting new features have raised questions that this thesis has sought to address by studying the impact of EVs on DCMG through load flow analysis.

The study begins with an exploration of EV charging dynamics. To achieve the goals of this thesis, a comprehensive model was developed, combining a stochastic model and a load flow model. They both have been reviewed through a state-of-the-art of their interest and the global interest of the thesis.

The system studied is complex and depends on many parameters such that an important list of scenarios has been dressed to evaluate the different aspects that could be encountered. They are based on simple architectures that constitute base cases on which the addition of EVCS is simulated with different load profiles.

The presentation of the results is segmented into four distinguished parts, all focusing on specific aspects. It was first necessary to understand how the DCMG reacts to simple variations and make a behaviour analysis of it. These observations have been extrapolated and associated with people's socio-cultural behaviour and technical changes.
The impact of the segregation between the CC and CP modes which is specific to the charging of EV batteries has been reviewed thoroughly. It concluded that the CC power

mode is more beneficial and can enhance the performance of the DCMG.
Having enough material to fully understand all the subtleties of EV charging, they have been added to the model in order to study their impact directly. This has been done by comparing the results of their addition to the base cases where they had not yet been added. The variables analyzed were intended to provide substances to the question of stability, independence and limitations of the DCMG.
Forecasts of the situation expected in Belgium for the year 2030 as a result of company car policies were finally simulated to evaluate future challenges and requirements.

Key findings suggest that both vehicle owners and grid operators benefit from avoiding overcharging EV batteries to prevent them from reaching the CP mode. This practice is harmful both for the battery life and microgrid performance.

The analysis of maximum currents revealed that while EVCS can moderate and have a positive impact on the limitations of the DCMG, they can also impose significant stress, necessitating larger line cross-sections.
Voltage stability tends to be moderately compromised by the EVCS while the grid independence suffers from these new arrivals as the number of interactions increases.

Projections for 2030 highlight the severe work that will be necessary for current existing MGs to be able to welcome the future fleet of company cars. This also indicates that it will not be possible to remain as independent as it is currently from the main grid without extensive, and often impractical, additions of PV capacity. Another technology could provide an additional source of energy, but it would probably be AC generation, which would reduce the interest in a DCMG.

In conclusion, while general trends were identified, the study acknowledges significant variability in the impact of EVs on different DCMGs due to the system's complexity. It is difficult to draw unanimous conclusions for all the different DCMGs that can exist. The ultimate effect will depend heavily on the design and sizing of the existing DCMG and the integration strategy for EVCS. When managed smartly, a moderate number of EVs, especially operating in CC mode, can be beneficial. However, without careful planning, the integration of EVs could have detrimental effects on DCMG performance.

Future work

Although this thesis aims to be as complete and detailed as possible, some assumptions and simplifications have been made. It would be interesting to verify if the results are confirmed while completely implementing the sophistication of EV charging.

Despite being grounded in practical data, the architecture of the base cases is based on assumptions, even though efforts were made to reflect realistic scenarios. A valuable next step would be to collect data from several existing MGs and run the same simulations on them to draw conclusions specific to those systems.

Finally, collaborating with a data scientist to conduct a large number of simulations and analyze the correlations between various factors such as microgrid architectures, energy balance and the placement of EVCS could yield some interesting observations. This approach would help establish the most effective strategies for implementing a DCMG that can efficiently accommodate an EVCS parking area.
The ultimate goal would be to develop a model capable of providing the optimal sizing and location of EVCS based on a given DCMG architecture.

Declaration of Generative AI and AI-assisted technologies in the writing process

During the preparation of this work the author used ChatGPT to refine the phrasing and structure of the text. After using this tool, the author reviewed and edited the content as needed and takes full responsibility for the content of the publication.

Appendices

Appendix A: Stochastic model

This appendix presents the details of the stochastic model and offers a qualitative validation of it through a visual comparison of the obtained plots. The parameters presented are the same as those of the document on which this appendix is based [19].

Parameters

Important parameters are the numbers of arrival, departure and total number of vehicles present at the parking area. Unfortunately, they are not provided but they have been retrieved from the provided graph illustrated in Figure 5.1 thanks to the tool 'PlotDigitizer' [39].

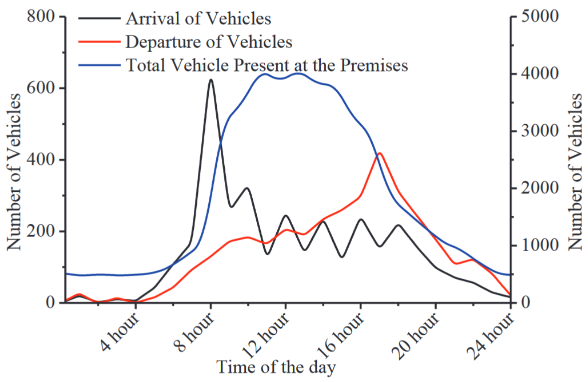

Figure 5.1: Arrival, departure and total number of vehicles present at the parking area

- $T_S = 15$ min = Time step
- $V_T(0) = 500$ = Total vehicle present at the charging station at the time $t = 0$
- ρ_{1i} = Correlation coefficient between the previous day's SOC and driving distance. It's computed from the following covariance matrix : $\begin{bmatrix} 1 & 0.5 \\ 0.5 & 1 \end{bmatrix}$

- ρ_{2i} = Correlation coefficient between SOC at time t^- and SOC of the departing vehicles. It's computed from the following covariance matrix : $\begin{bmatrix} 1 & 1 \\ 1 & 1 \end{bmatrix}$
- ρ_{3i} = Correlation coefficient between SOC at time t and SOC of arriving vehicles. It's computed from the following covariance matrix : $\begin{bmatrix} 1 & 0.75 \\ 0.75 & 1 \end{bmatrix}$
- M_i = [1/8, 1/8, 1/8, 1/8, 1/8, 1/8, 1/8, 1/8] = Market share
- P_C = [1.4, 1.5, 3.3, 3.3, 3.3, 3.3, 3.3, 6.6] kW = Charging power
- μ_d = [1.6, 3.2, 12.8, 16, 36.2, 36.2, 36.2, 36.2] km = Mean of driving distance between home and workplace
- σ_d = [0.9, 1.8, 7, 8.9, 19.9, 19.9, 19.9, 19.9] km = Standard deviation of driving distance between home and workplace
- S_B = [4, 8, 16, 22, 24, 27, 28, 53] kWh = Battery size
- d_R = [8, 16, 64, 80, 160, 190, 251, 354] km = Driving range
- $K = 25\%$ = Penetration of EVs
- $\mu_{Di}^{PD} = 80\%$ = Mean SOC of previous day's departure
- $\sigma_{Di}^{PD} = 16\%$ = standard deviation SOC of previous day's departure
- $s_i = 100\%$ = Charging set-point or charging efficiency
- $\mu_i(0^+) = 70\%$ = Mean initial SOC at the charging station
- $\sigma_i(0^+) = 16\%$ = standard deviation of the initial SOC at the charging station

To provide clarity and to give an intuitive understanding of which parameter corresponds to which kind of vehicle, Figure 5.2 illustrates the composition of the vehicle fleet where each type constitutes the market share that is assigned to them.

It's also good to note that the normal distribution of arrival SOC (X_{AI}) is slightly different from the one presented in the paper in Equation 2.2 as it's bounded but this equation was not mentioned in the report for the lightness of writing. The actual mean of SOC on arrival (μ_{Ai}) can be computed by using the CDF and PDF which are respectively represented by Φ_{Ai} and ϕ_{Ai} in the following equation :

$$\begin{aligned} \mu_{Aai} = a_{Ai}\Phi_{Ai}(a_{Ai}) + b_{Ai}(1 - \Phi_{Ai}(b_{Ai}))+ \\ \mu_{Ai}(\Phi_{Ai}(b_{Ai}) - \Phi_{Ai}(a_{Ai})) - \sigma_{Ai}^2(\phi_{Ai}(b_{Ai}) - \phi_{Ai}(a_{Ai})) \end{aligned} \tag{5.1}$$

where $a_{Ai} = 20\%$ and $b_{Ai} = 90\%$.

Company	Model	EV Types	Driving Range (km)	Battery Size (kWh)
Toyota	Prius	PHEV	8	4
Buick		PHEV	16	8
Chevrolet	Volt	EREV	64	16
Fisker	Karma	PHEV	80	22
Nissan	LEAF	EV	160	24
Toyota	RAV4	EV	190	27
Cooper	Mini E	EV	251	28
Tesla	Roadster	EV	354	53

Figure 5.2: Different EVs and their characteristics

Model validation

The plots obtained from the implemented model are compared with the results presented in the paper. It can be seen that the plot of the power demands from the paper (on the

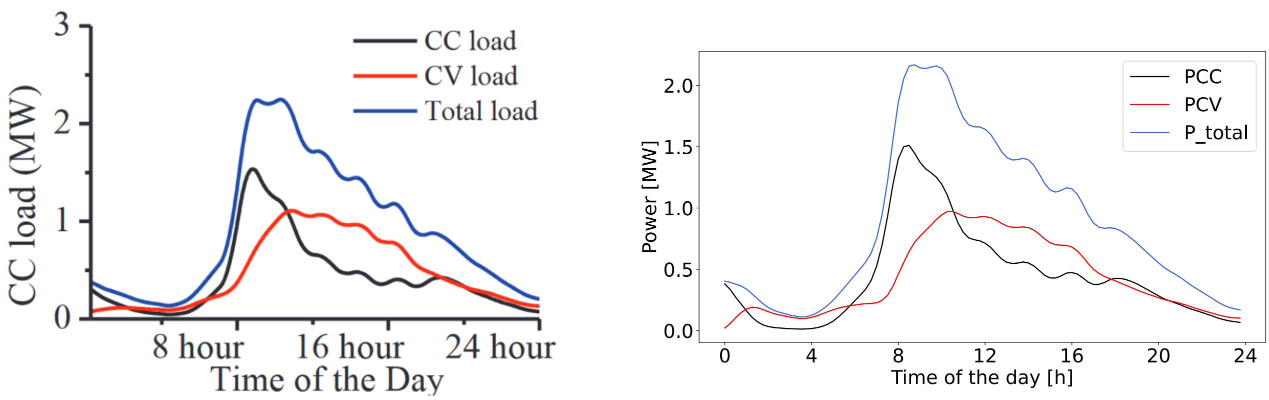

Figure 5.3: Predicted daily CC, CV, and total load profiles

left) is the same as those in the implemented model (on the right) It can be observed that the plot of the SOC delivered from the paper (on the left) is the same as that in the implemented model (on the right

Appendix B : Scenarios

This appendix is segmented into two parts. The first section is about the justifications and assumptions taken to size and design the various scenarios and their variables. The second part provides a detailed presentation of these variables with numerical values.

Justifications and assumptions

Industrial load

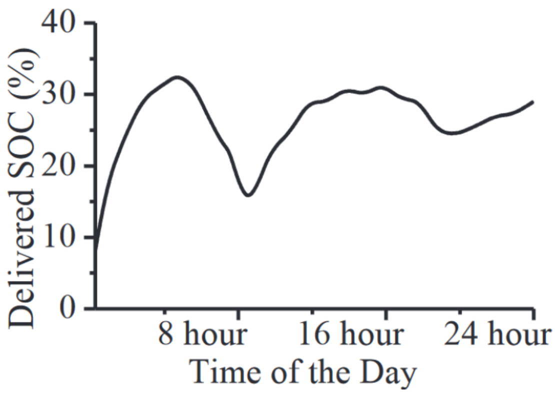

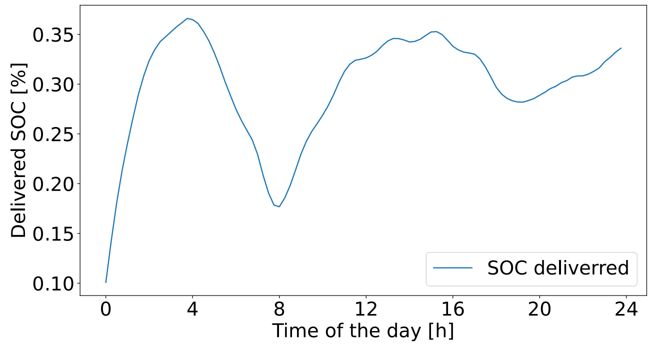

Figure 5.4: Delivered SOC

The industrial loads were provided by the teaching staff and were not modified. Eight choices were available but the choice of this precise load was made based on criteria such as high maximum power and a minimum power consumption that was not too low compared to the total energy requirement for the year. It's the load that behaved most like an office where people primarily work on computers.
Assuming that this industrial load corresponds to an office environment, the number of people working there can be estimated by using the average consumption of a worker at his workplace. According to data from [40], the average consumption is estimated to be 2 MWh/year for an office space of $10m^2$ per person.
Given the total energy requirement per year of 315 MWh, it can be calculated that approximately 157 people are working in this office space.
The load profile for the first week of the year is shown for illustrative purposes.

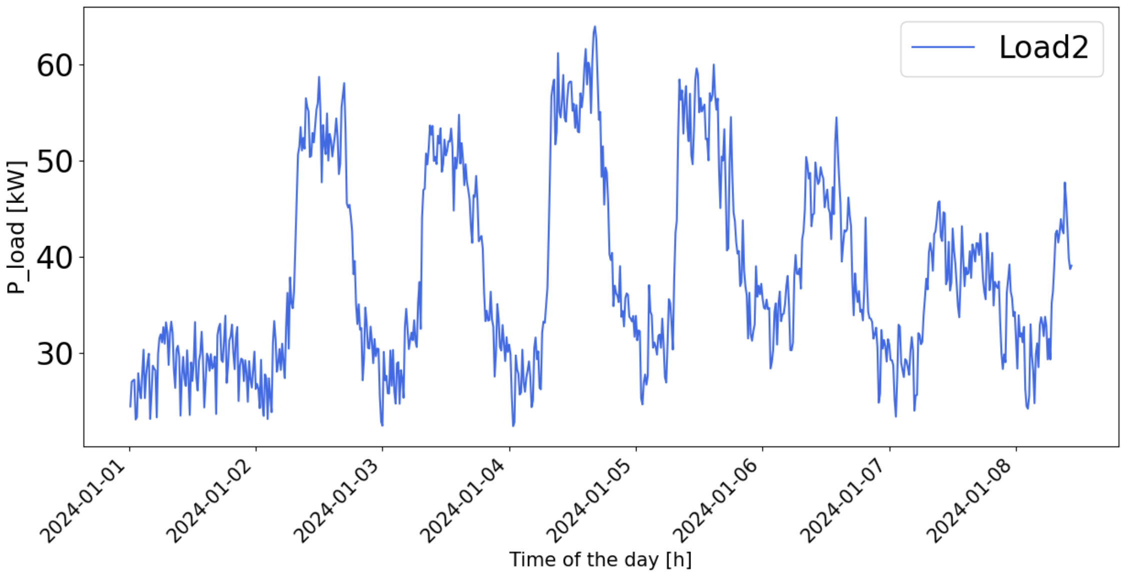

Figure 5.5: Load profile of the industrial load for the first week of the year

EVs charging station

The 'weekday' and 'punctual' profiles for arrival, departure and total number of vehicles present in the parking area as shown in Figure 3.1 and in Figure 3.3 are designed such that the peak number of vehicles present in the charging station doesn't exceed 157 people which corresponds to the computed number of workers.

Pv panels

The company building is designed to welcome roughly 160 people. It's a reasonable assumption to suppose that they are distributed across 4 floors. Considering 40 people per floor and 10 square meters of office space per worker, it gives $400m^2$ per floor.
Taking into account the common areas (toilets, corridors, cafeteria, etc.), the available surface can be assumed to be increased by 50%, totaling a surface of 600 square meters per floor and, logically, the same surface is available on the roof.
However, not all of this available roof space can be effectively utilized for PVs due to the need for optimization through inclination. Indeed, as a flat roof is supposed, PVs have to be inclined to optimize their production. With a typical optimum angle of 30° [41] for PVs on a flat roof, a spacing of twice the height of the PVs between rows [42] and given that the usual dimension of a PV is 1.6 x 1m, it gives that $1 * sin(30) = 0.5m$ so two times this distance gives 1 meter between each row of PVs. Finally, it's estimated that 225 PVs can be installed on the roof of the building.
Similarly, considering an estimated 8 square meters of available roof space per vehicle in the parking area, approximately 525 PVs can be installed over the parking spots using the same approach.
It gives a total of 750 PVs which act as a non-dispatchable DG unit for the DCMG.

Battery

It's a common practice to size a fixed battery to hold approximately 10 hours of average consumption to provide energy during the night, especially when the source of production is solar dependent. Considering that the mean power consumption on the grid due to the various loads is approximately $60kW$, a capacity of $600kWh$ is needed. Moreover, the chosen battery capacity aligns well with the size of the building, considering the volumetric size and weight of the battery. According to data available from Sungrow's site [43] regarding their product, it's estimated that their battery achieves a volumetric energy density of $117.25kWh/m^3$ and a mass-energy density of $118kWh/t$. Based on these figures, the battery would occupy a volume of approximately $5.11m^3$ and weigh around $5.1t$, which appears acceptable.
Regarding the (dis-)charging rate, a typical value for batteries of this size is around four hours.

Line cross section

The computation of the line cross section was performed using an online calculator [44] with the most extreme parameters as input. These extreme values were observed during the 'Punctual&weekend' simulation and are as follows :
$V = 700V$, $\Delta V = 5\%$, $L = 400m$, $I = 225A$.
It gives a minimum cross-section of $118mm^2$. Considering several predefined existing cross-section options, the closest higher value to this calculated minimum is $120mm^2$. This choice results in a resistance of $0.153\Omega/km$, as provided by [36].

Bibliography

[1] *CO2 Emissions in 2022 – Analysis*, en-GB. [Online]. Available: https://www.iea.org/reports/co2-emissions-in-2022 (visited on 03/11/2024).

[2] R. Asad and A. Kazemi, "A novel decentralized voltage control method for direct current microgrids with sensitive loads," en, *International Transactions on Electrical Energy Systems*, vol. 25, no. 2, pp. 197–215, 2015, _eprint: https://onlinelibrary.wiley.com/doi/p ISSN: 2050-7038. DOI: 10.1002/etep.1833. [Online]. Available: https://onlinelibrary.wiley.com/doi/abs/10.1002/etep.1833 (visited on 03/12/2024).

[3] A. Maulik and D. Das, "Application of linearised load flow method for droop-controlled DCMGs," en, *IET Generation, Transmission & Distribution*, vol. 14, no. 6, pp. 1114–1126, 2020, _eprint: https://onlinelibrary.wiley.com/doi/pdf/10.1049/iet-gtd.2018.7113, ISSN: 1751-8695. DOI: 10.1049/iet-gtd.2018.7113. [Online]. Available: https://onlinelibrary.wiley.com/doi/abs/10.1049/iet-gtd.2018.7113 (visited on 02/16/2024).

[4] *Charging infrastructures for EV: Overview of technologies and issues | IEEE Conference Publication | IEEE Xplore*. [Online]. Available: https://ieeexplore.ieee.org/abstract/document/6387434?casa_token=y1WzNaZ7AkIAAAAA:zenK-VBxwWSy1Ga04HpEXSlqz-HLx5jjFx7wvIzKLFR4fIqSZsblx8iCsUHqg03tif-sSZkVD543Pi0 (visited on 04/03/2024).

[5] *Que signifient les acronymes BEV, HEV, PHEV, FCEV et EREV ? - bornes-recharges.fr*, fr-FR, Section: Bornes de recharges pour voitures, Mar. 2024. [Online]. Available: https://bornes-recharges.fr/que-signifient-les-acronymes-bev-hev-phev-fcev-et-erev/ (visited on 05/14/2024).

[6] leyicase168@gmail.com, *Difference between AC and DC chargers*, en. [Online]. Available: https://www.soonplus-ev.com/news/ac-vs-dc-chargers/ (visited on 04/14/2024).

[7] *The Four EV Charging Modes in the IEC 61851 Standard - Technical Articles*. [Online]. Available: https://www.allaboutcircuits.com/technical-articles/four-ev-charging-modes-iec61851-standard/ (visited on 04/14/2024).

[8] *ChargePoint Introduces New 500 kW Ultra-Fast DC Charging System*. [Online]. Available: https://insideevs.com/news/696420/chargepoint-500kw-dc-fast-charging-system/ (visited on 04/14/2024).

[9] H. D. Young, R. A. Freedman, and A. L. Ford, *University Physics with Modern Physics*, 13th. University Physics with Modern Physics, 2011.

[10] *2021 Tesla Model 3 LR AWD With 82 kWh Battery: Charging Analysis*, en. [Online]. Available: https://insideevs.com/news/519382/tesla-model3-82kwh-charging-analysis/ (visited on 04/14/2024).

[11] *Kia EV6 Prototype Fast Charging Analysis: Very Fast But Quirky*, en. [Online]. Available: https://insideevs.com/news/537223/kia-ev6-prototype-fast-charging/ (visited on 04/14/2024).

[12] K. Qian, C. Zhou, M. Allan, and Y. Yuan, "Modeling of Load Demand Due to EV Battery Charging in Distribution Systems," *IEEE Transactions on Power Systems*, vol. 26, no. 2, pp. 802–810, May 2011, Conference Name: IEEE Transactions on Power Systems, ISSN: 1558-0679. DOI: 10.1109/TPWRS.2010.2057456. [Online]. Available: https://ieeexplore.ieee.org/abstract/document/5535237 (visited on 04/14/2024).

[13] M. S. ElNozahy and M. M. A. Salama, "A Comprehensive Study of the Impacts of PHEVs on Residential Distribution Networks," *IEEE Transactions on Sustainable Energy*, vol. 5, no. 1, pp. 332–342, Jan. 2014, Conference Name: IEEE Transactions on Sustainable Energy, ISSN: 1949-3037. DOI: 10.1109/TSTE.2013.2284573. [Online]. Available: https://ieeexplore.ieee.org/document/6674071 (visited on 04/14/2024).

[14] K. Clement-Nyns, E. Haesen, and J. Driesen, "The Impact of Charging Plug-In Hybrid Electric Vehicles on a Residential Distribution Grid," *IEEE Transactions on Power Systems*, vol. 25, no. 1, pp. 371–380, Feb. 2010, Conference Name: IEEE Transactions on Power Systems, ISSN: 1558-0679. DOI: 10.1109/TPWRS.2009.2036481. [Online]. Available: https://ieeexplore.ieee.org/document/5356176 (visited on 04/14/2024).

[15] A. M. A. Haidar and K. M. Muttaqi, "Behavioral Characterization of Electric Vehicle Charging Loads in a Distribution Power Grid Through Modeling of Battery Chargers," *IEEE Transactions on Industry Applications*, vol. 52, no. 1, pp. 483–492, Jan. 2016, Conference Name: IEEE Transactions on Industry Applications, ISSN: 1939-9367. DOI: 10.1109/TIA.2015.2483705. [Online]. Available: https://ieeexplore.ieee.org/abstract/document/7283610?casa_token=QJvqeyb8xBkAAAAA:HElNK_IF_Ku6vclp1hWWX33yEF1tKPEbkMYqIwoEHQCDIZ8KfvKziQHX70S0ZO (visited on 04/14/2024).

[16] H. Mehrjerdi and R. Hemmati, "Stochastic model for electric vehicle charging station integrated with wind energy," *Sustainable Energy Technologies and Assessments*, vol. 37, p. 100 577, Feb. 2020, ISSN: 2213-1388. DOI: 10.1016/j.seta.2019.100577. [Online]. Available: https://www.sciencedirect.com/science/article/pii/S2213138819304199 (visited on 04/14/2024).

[17] R.-C. Leou, C.-L. Su, and C.-N. Lu, "Stochastic Analyses of Electric Vehicle Charging Impacts on Distribution Network," *IEEE Transactions on Power Systems*, vol. 29, no. 3, pp. 1055–1063, May 2014, Conference Name: IEEE Transactions on Power Systems, ISSN: 1558-0679. DOI: 10.1109/TPWRS.2013.2291556. [Online]. Available: https://ieeexplore.ieee.org/document/6678651/references#references (visited on 04/14/2024).

[18] F. Marra, G. Y. Yang, C. Træholt, E. Larsen, C. N. Rasmussen, and S. You, "Demand profile study of battery electric vehicle under different charging options," in *2012 IEEE Power and Energy Society General Meeting*, ISSN: 1944-9925, Jul. 2012, pp. 1–7. DOI: 10.1109/PESGM.2012.6345063. [Online]. Available: https://ieeexplore.ieee.org/document/6345063 (visited on 04/14/2024).

[19] M. S. Islam and N. Mithulananthan, "Daily ev load profile of an ev charging station at business premises," in *2016 IEEE Innovative Smart Grid Technologies - Asia (ISGT-Asia)*, 2016, pp. 787–792. DOI: 10.1109/ISGT-Asia.2016.7796485.

[20] B. S. Publication, *BS EN 61851-23:2014 Electric vehicle conductive charging system*, Part 23. DC Electric Vehicle Charging Station, 2014.

[21] A. Garces, "A Linear Three-Phase Load Flow for Power Distribution Systems," *IEEE Transactions on Power Systems*, vol. 31, no. 1, pp. 827–828, Jan. 2016, Conference Name: IEEE Transactions on Power Systems, ISSN: 1558-0679. DOI: 10.1109/TPWRS.2015.2394296. [Online]. Available: https://ieeexplore.ieee.org/document/7027253 (visited on 04/14/2024).

[22] O. D. Montoya, L. F. Grisales-Noreña, D. González-Montoya, C. A. Ramos-Paja, and A. Garces, "Linear power flow formulation for low-voltage DC power grids," *Electric Power Systems Research*, vol. 163, pp. 375–381, Oct. 2018, ISSN: 0378-7796. DOI: 10.1016/j.epsr.2018.07.003. [Online]. Available: https://www.sciencedirect.com/science/article/pii/S0378779618301962 (visited on 04/14/2024).

[23] O. D. Montoya, "On Linear Analysis of the Power Flow Equations for DC and AC Grids With CPLs," *IEEE Transactions on Circuits and Systems II: Express Briefs*, vol. 66, no. 12, pp. 2032–2036, Dec. 2019, Conference Name: IEEE Transactions on Circuits and Systems II: Express Briefs, ISSN: 1558-3791. DOI: 10.1109/TCSII.2019.2894149. [Online]. Available: https://ieeexplore.ieee.org/document/8620316 (visited on 04/14/2024).

[24] R. Asad and A. Kazemi, "A novel slack bus-free load flow method for dc microgrids and distribution systems with dc-bus signaling control methods," *International Transactions on Electrical Energy Systems*, vol. 25, no. 12, pp. 3538–3552, 2015. DOI: https://doi.org/10.1002/etep.2050. eprint: https://onlinelibrary.wiley.com/doi/pdf/10.1002/etep.2050. [Online]. Available: https://onlinelibrary.wiley.com/doi/abs/10.1002/etep.2050.

[25] R. Farooq, L. Mateen, M. Ahmad, S. Q. Akbar, H. A. Khan, and N. A. Zaffar, "Smart DC microgrids: Modeling and power flow analysis of a DC Microgrid for off-grid and weak-grid connected communities," in *2014 IEEE PES Asia-Pacific Power and Energy Engineering Conference (APPEEC)*, ISSN: 2157-4847, Dec. 2014, pp. 1–6. DOI: 10.1109/APPEEC.2014.7066139. [Online]. Available: https://ieeexplore.ieee.org/document/7066139 (visited on 04/14/2024).

[26] P. Kundur, N. J. Balu, and M. G. Lauby, *Power System Stability and Control*. New York: McGraw-Hill, 1994, vol. 7.

[27] O. A. Afolabi, W. H. Ali, P. Cofie, J. Fuller, P. Obiomon, and E. S. Kolawole, "Analysis of the Load Flow Problem in Power System Planning Studies," en, *Energy and Power Engineering*, vol. 7, no. 10, pp. 509–523, Sep. 2015, Number: 10 Publisher: Scientific Research Publishing. DOI: 10.4236/epe.2015.710048. [Online]. Available: https://www.scirp.org/journal/paperinformation.aspx?paperid=60124 (visited on 04/05/2024).

[28] K. S. Musti and R. B. Ramkhelawan, "Power system load flow analysis using microsoft excel," *Spreadsheets in Education*, vol. 6, no. 1, 2012.

[29] A. Elrayyah, Y. Sozer, and M. E. Elbuluk, "A Novel Load-Flow Analysis for Stable and Optimized Microgrid Operation," *IEEE Transactions on Power Delivery*, vol. 29, no. 4, pp. 1709–1717, Aug. 2014, Conference Name: IEEE Transactions on Power Delivery, ISSN: 1937-4208. DOI: 10.1109/TPWRD.2014.2307279. [Online]. Available: https://ieeexplore.ieee.org/abstract/document/6774974?casa_token=jZpWltbMIfQAAAAA:ODf-_Zl1FXcR5v6pie-6HtrIl0BZBhLfFEzD5_syzadz2bn_jcvaXvTKhZm10OCOq0XMMrqM5Bj_5eI (visited on 04/05/2024).

[30] A. Esmaeli, M. Abedini, and M. H. Moradi, "A novel power flow analysis in an islanded renewable microgrid," *Renewable Energy*, vol. 96, pp. 914–927, Oct. 2016, ISSN: 0960-1481. DOI: 10.1016/j.renene.2016.04.077. [Online]. Available: https://www.sciencedirect.com/science/article/pii/S0960148116303792 (visited on 04/05/2024).

[31] B. Dağ, A. R. Boynueğri, Y. Ateş, A. Karakaş, A. Nadar, and M. Uzunoğlu, "Static Modeling of Microgrids for Load Flow and Fault Analysis," *IEEE Transactions on Power Systems*, vol. 32, no. 3, pp. 1990–2000, May 2017, Conference Name: IEEE Transactions on Power Systems, ISSN: 1558-0679. DOI: 10.1109/TPWRS.

2016.2613547. [Online]. Available: https://ieeexplore.ieee.org/abstract/document/7576668?casa_token=Dou3aUGWCs4AAAAA:ZibZXHLnj87Q8R9Yk0wNCt76fOgpV3TIVD
(visited on 04/05/2024).

[32] R. Farooq, L. Mateen, M. Ahmad, S. Q. Akbar, H. A. Khan, and N. A. Zaffar, "Smart DC microgrids: Modeling and power flow analysis of a DC Microgrid for off-grid and weak-grid connected communities," in *2014 IEEE PES Asia-Pacific Power and Energy Engineering Conference (APPEEC)*, ISSN: 2157-4847, Dec. 2014, pp. 1–6. DOI: 10.1109/APPEEC.2014.7066139. [Online]. Available: https://ieeexplore.ieee.org/abstract/document/7066139?casa_token=V2Qyx6P1U5oAAAAA:WKljDr3-LNFjIcn3sokCGnTRltfPqUiJMjzKySbFa35zUASEtEUpbtn8DiHX6m
(visited on 04/05/2024).

[33] C. Li, S. K. Chaudhary, M. Savaghebi, J. C. Vasquez, and J. M. Guerrero, "Power Flow Analysis for Low-Voltage AC and DC Microgrids Considering Droop Control and Virtual Impedance," *IEEE Transactions on Smart Grid*, vol. 8, no. 6, pp. 2754–2764, Nov. 2017, Conference Name: IEEE Transactions on Smart Grid, ISSN: 1949-3061. DOI: 10.1109/TSG.2016.2537402. [Online]. Available: https://ieeexplore.ieee.org/abstract/document/7442160?casa_token=iypWw8O1-VgAAAAA:HOpUe1kOSnaGD-lvttieuAUGJb6dai7b2iUueIkL1AlLOyuOfloMmKeMiBNuUtLTlux_YXwmmr6Y7FQ (visited on 04/05/2024).

[34] D. Wang, F. Locment, and M. Sechilariu, "Modelling, Simulation, and Management Strategy of an Electric Vehicle Charging Station Based on a DC Microgrid," en, *Applied Sciences*, vol. 10, no. 6, p. 2053, Jan. 2020, Number: 6 Publisher: Multidisciplinary Digital Publishing Institute, ISSN: 2076-3417. DOI: 10.3390/app10062053. [Online]. Available: https://www.mdpi.com/2076-3417/10/6/2053 (visited on 04/08/2024).

[35] K. Sayed, A. G. Abo-Khalil, and A. S. Alghamdi, "Optimum Resilient Operation and Control DC Microgrid Based Electric Vehicles Charging Station Powered by Renewable Energy Sources," en, *Energies*, vol. 12, no. 22, p. 4240, Jan. 2019, Number: 22 Publisher: Multidisciplinary Digital Publishing Institute, ISSN: 1996-1073. DOI: 10.3390/en12224240. [Online]. Available: https://www.mdpi.com/1996-1073/12/22/4240 (visited on 04/08/2024).

[36] "Appendix 4 - Cable Data-Resistance, Impedance and 'R1 + R2' Values," en, in *Guide to the Wiring Regulations*, _eprint: https://onlinelibrary.wiley.com/doi/pdf/10.1002/978047
John Wiley & Sons, Ltd, 2008, pp. 272–275, ISBN: 978-0-470-99837-3. DOI: 10.1002/9780470998373.app4. [Online]. Available: https://onlinelibrary.wiley.com/doi/abs/10.1002/9780470998373.app4 (visited on 05/12/2024).

[37] S. Singh, A. R. Gautam, and D. Fulwani, "Constant power loads and their effects in DC distributed power systems: A review," *Renewable and Sustainable Energy*

Reviews, vol. 72, pp. 407–421, May 2017, ISSN: 1364-0321. DOI: 10.1016/j.rser.2017.01.027. [Online]. Available: https://www.sciencedirect.com/science/article/pii/S1364032117300412 (visited on 05/21/2024).

[38] *Calcul de section de câble électrique. Formule de calcul de section de câble suivant l'intensité ou la puissance.* [Online]. Available: https://schema-electrique.net/calcul-section-cable-electrique-formule-intensite-puissance.html (visited on 05/26/2024).

[39] *PlotDigitizer*, https://plotdigitizer.com/app.

[40] *Évaluer les consommations d'un local de bureau*, fr-FR. [Online]. Available: https://energieplus-lesite.be/evaluer/energie-et-les-consommations2/evaluer-les-consommations-d-un-local-de-bureau/ (visited on 05/13/2024).

[41] T. Solaire, *Panneau solaire : Inclinaison & orientation optimales [2020]*, fr-FR, Mar. 2023. [Online]. Available: https://terresolaire.com/Blog/batiment-solaire/inclinaison-panneau-solaire-orientation/ (visited on 05/13/2024).

[42] Sébastien, *Le guide de l'installation photovoltaïque sur toiture plate*, fr_FR, Section: Installation Solaire, Jul. 2022. [Online]. Available: https://solaire-france.com/panneaux-solaires-toit-plat/ (visited on 05/13/2024).

[43] *Product | SUNGROW.* [Online]. Available: https://fra.sungrowpower.com/productDetail/2821 (visited on 05/13/2024).

[44] *Calcul Section Câble : Calculez facilement votre section de fil*, fr-FR, Oct. 2020. [Online]. Available: https://commentcalculer.fr/calcul/section-cable/ (visited on 05/13/2024).

UNIVERSITÉ CATHOLIQUE DE LOUVAIN
École polytechnique de Louvain
Rue Archimède, 1 bte L6.11.01, 1348 Louvain-la-Neuve, Belgique | **www.uclouvain.be/epl**